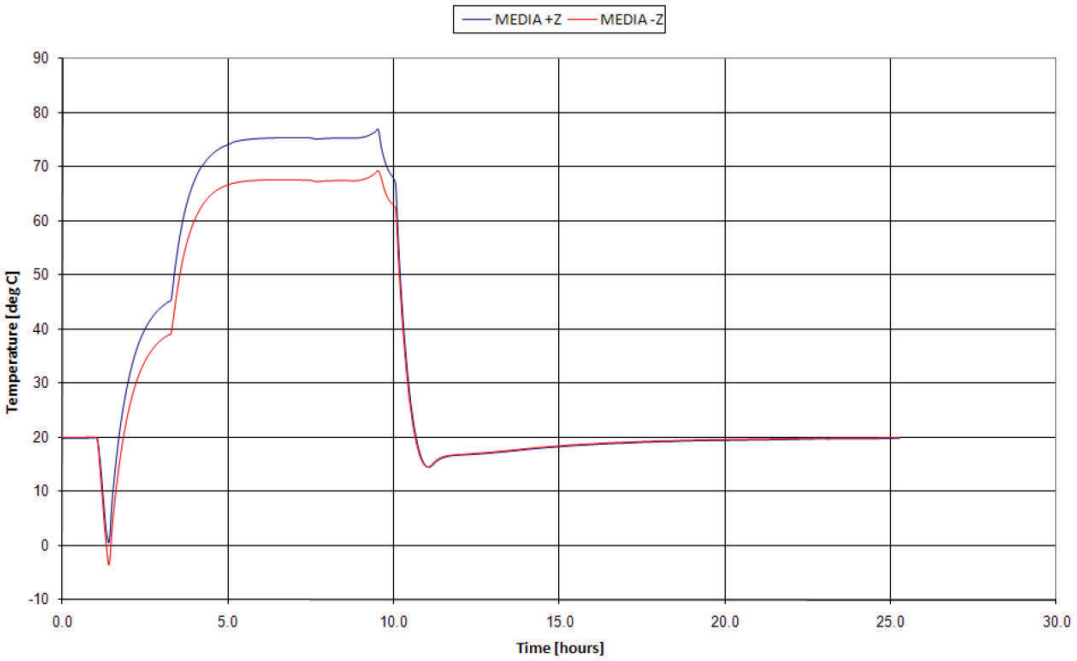


Figure 4.7: Temperatures during ABB test case 2.

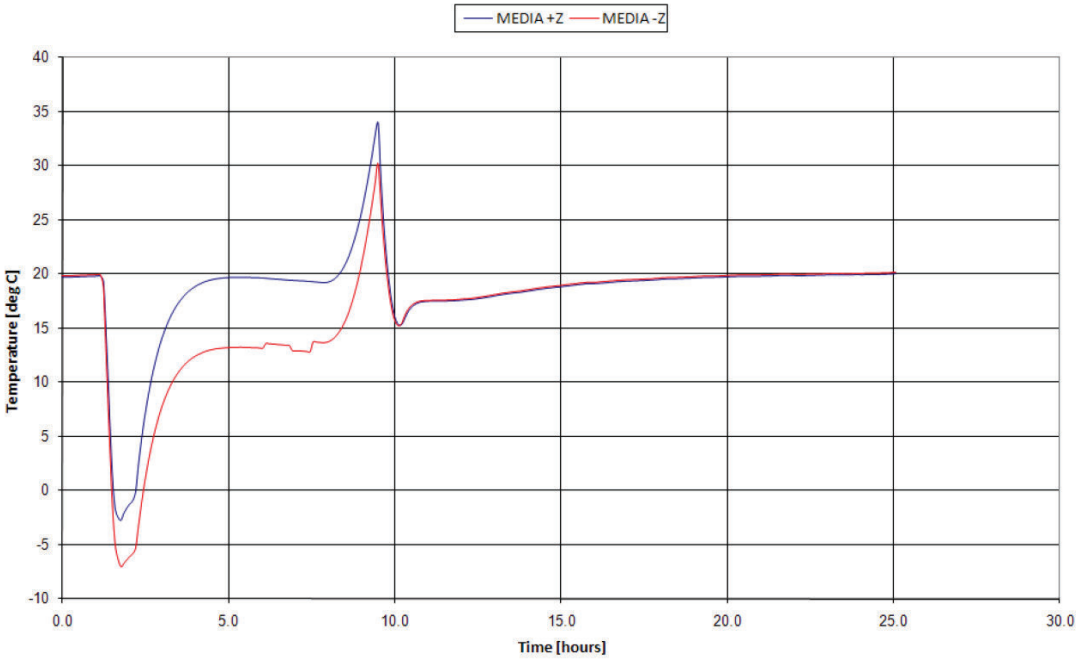


Figure 4.8: Temperatures during ABB test case 3.

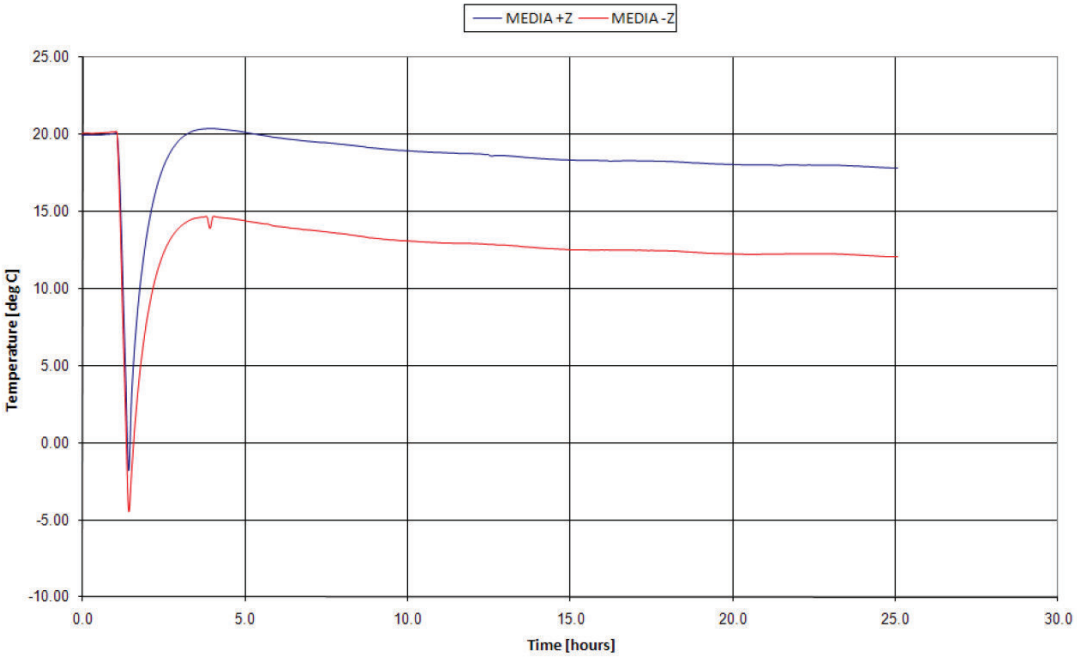


Figure 4.9: Temperatures during ABB test case 4.

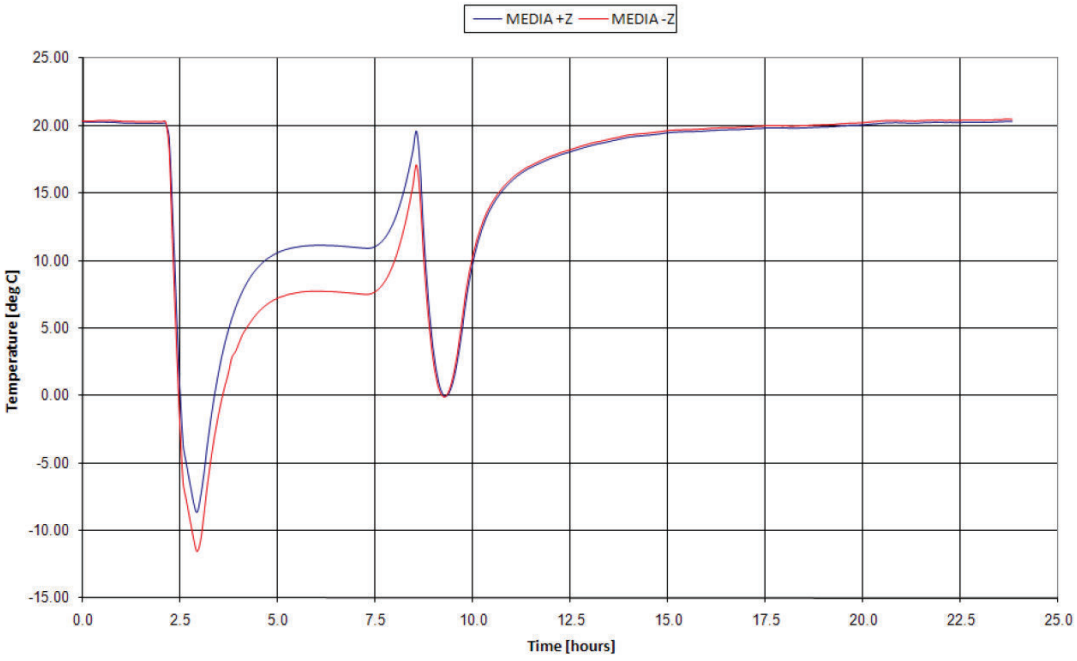


Figure 4.10: Temperatures during ABB test case 5.

Table 4.2: ABB C/C panel conductivity values (automatic TMM correlation).

| **Method** | $k_x$ **(W/m/K)** | $k_y$ **(W/m/K)** | $k_z$ **(W/m/K)** |
|---|---|---|---|
| DoE | 48.858 | 48.858 | 1.7 |
| DoE | 40.46 | 52.8 | 1.53 |
| Downhill Simplex | 54.99 | 46.28 | 1.4 |
| NLPQL | 49.72 | 47.28 | 1.4 |

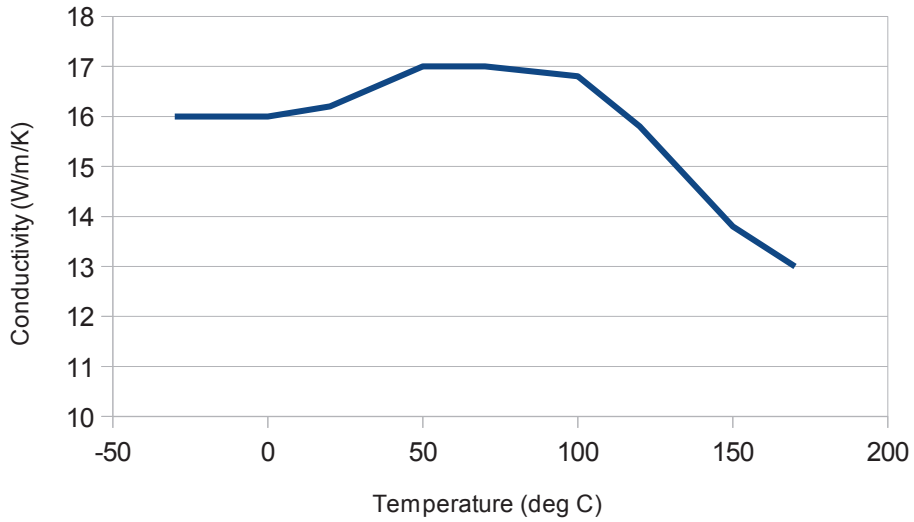


Figure 4.11: Carbon-Carbon through-the-thickness conductivity measured at SERMS Lab.

It is worth noticing that, abandoning the hypothesis of panel isotropy, and thanks to the automatic optimization, it was possible to obtain a much better correlation. This opens the door to a series of hypothesis: the ribbons in the C/C honeycomb core (or the adhesive stripes used to bond skins and core together) could create a preferential heat path and therefore justify different values for $k_x$ and $k_y$.

Moreover, it is interesting to notice that, from tests conducted at the SERMS Lab (Terni, Italy) on a smaller sandwich sample with a similar core density, the thermal conductivity in the through-the-thickness direction is much higher that that extrapolated from prototype level TVT. As can be seen in Figure 4.11, values in the TVT temperature range are around $16 \div 17$ W/m/K. This corroborates the hypothesis of process problems with scaled up panels that are probably not completely graphitized.

However, even with a concentrated power dissipation layout and despite the manufacturing problems that led to low conductivity values, the heat rejection capability of the panel is still interesting if compared with the performance of standard aluminium radiator panels with embedded heat pipes ($\sim 300\ W/m^2$). For

the reference configuration of Case 2 (total power: 190 W; H1, H3, H5 at 50 W; H2, H4 at 20 W) and a maximum experimental temperature of 77°C (spot on H5 heater; all electronics within temperature limits) the ABB heat reject capability is:

$$\frac{Q}{A} = \frac{190}{0.5} = 380\frac{W}{m^2} \tag{4.1}$$

where $Q$ is the power dissipation and $A$ is the radiating area.

Apart from considerations on the thermal conductivity, the thermal vacuum test proved the ability of the commercial components to survive high vacuum and thermal cycling, while still behaving consistently. The flexible circuitry was bonded to the Carbon-Carbon through the two-component epoxy adhesive system made by Araldite®AV138M with hardener HV998. This material was chosen because:

- It is already space qualified.
- It has low outgassing with TML = 0.84%, RML =0.57%, CVCM = 0.02% according to ECSS-Q-70-02[1] and passed NASA NHB 8060-1A test for toxicity and offgassing, which makes it suitable for specialist electronic, telecommunication, and aerospace applications.
- It presents excellent chemical resistance and good temperature resistance (up to 120 °C as long term exposure)
- It passed NASA NHB 8060-1B 24.5% O2 flammability test.
- Being a thixotropic paste, it has good gap filling properties, that can help improving bonding with the rough composite panel's surface.

The mix ratio of the two components (Araldite:hardener) was 100:40 by weight or volume (they have the same density), and the resulting adhesive had a specific gravity[2] of $\sim 1.7$ and a pot life of 35 minutes. Strength and durability of the bonded joint are highly dependant on the proper treatment of the surfaces to be bonded: to obtain the best results, joint surfaces should be made rough (by mechanical abrasion or chemical etching), and cleaned with a good quality degreasing agent. After the surfaces have dried, a thin ($0.05 \div 0.10$ mm) adhesive layer can be applied with a spatula, and matching components should be clamped together in a way that ensures even contact pressure. Therefore, the procedure for bonding flexible motherboards on the substrate started with an overall cleaning of the panel with isopropyl alcohol, then a paper mask was applied, and the shapes were transfered on the skin with a white pencil. Then, contours were highlighted with Teflon tape, and the selected spots were rubbed with thin sandpaper and cleaned with scrub sponge. The clean areas were then covered with a smooth, thin and regular layer of Araldite, spread with a spatula. Just after smoothing the glue, Teflon tape was removed and pieces were placed in their final position trying to avoid any trapped

[1] As a reminder, the general requirement for materials outgassing is RML $< 1.0\%$ and CVCM $< 0.1\%$.

[2] Specific gravity or relative density, according to ASTM D-792, is the dimensionless ratio of the density of a material at a given temperature to the density of an equal volume of deionized water at the same temperature, usually 23°C.

Table 4.3: Comparison of harness required for the ABB thermal vacuum test under the assumption of three different communication protocols. The first row is the configuration that was actually built and tested.

| **Technology** | **# of cables on test article** | **# of cables crossing feedthroughs** |
|---|---|---|
| OneWire + USB | 4 | 10 |
| OneWire | 4 | 4 |
| Analog thermocouples | 148 | 148 |

air under them. They were retained firmly by Teflon tape. A foam rubber layer was placed on the assembly and heavy masses were leant on the foam rubber, in order to uniformly distribute pressure and lead to an accurate hardening. The adhesive can cure at different T ($\sim 5 \div 100$ °C), and highest temperatures ensure better mechanical properties.

Masses were let in place for 36 hours and, following ESA's recommendations, the bonding was allowed to cure for 48 hours at room temperature. The result was thoroughly examined to check for minimal glue leakages and was found to be perfectly clean. The CTE of the final joint, in the range 18 °C and 93°C, was $67 \cdot 10^{-6}$ $K^{-1}$; thermal conductivity at 30°C was 0.35 W/m/K. The proper combination of adhesive and bonding procedure led to a joint capable of resisting TVT without damage, and overcame the disbonding problems experienced with previous prototypes.

It is important to notice that the paper mask aid used to transfer the flexible motherboards on the support panel is not simply an useful AIT tool. During design and development phases, paper dolls of the circuits, printed at a 1:1 scale, are essential instruments for fit checks, and to make sure bends, corners and connectors' positions are all correct.

Besides checking the great response of COTS electronics, flex substrates, and assembly procedures, the ABB TVT highlighted another positive characteristic of the ABB design. In fact, one of the advantages deriving from the use of distributed electronics connected via few-wires protocols is that the number of cables to be routed on the test article and outside the test chamber is relatively small. In general, the total number of connections is one order of magnitude less than the same case equipped with conventional TCs. ABB has two motherboards (21 sensors each) and two Dallas cables (16 sensors each), therefore there are 37+37=74 OneWire sensors. Choosing USB protocol to transfer data outside TVC, there are 5+5=10 wires crossing the feedthroughs. Choosing OneWire protocol to transfer data outside TVC, there would be 2+2=4 wires crossing the feedthroughs. Choosing conventional thermocouples there would be 74*2=148 wires crossing the feedthroughs (see Table 4.3 for a quick resume).

Summing up, referring to Table 4.4, and recalling various types of multifunctionality, one can notice that ABB has all the characteristics to be a complete MFS. Thermal, structural, electrical and health monitoring systems are all present in

Table 4.4: MFS based on the smart skin concept have threefold multifunctionality.

| **Type I Multifunctionality: Added Subsystems** |
|---|
| Subsystem addition to provide additional performance |
| Connectivity or links between subsystems |
| Increased physical or information coupling between subsystems |
| **Type II Multifunctionality: Co-located Components** |
| Component co-location to provide packaging integration |
| Reduced dimensionality and complexity of final system |
| Physical distances between subsystems are reduced |
| **Type III Multifunctionality: Integrated Materials** |
| Material Selection based on a set of properties to satisfy more than one subsystem function |
| Physical volumes of subsystems are combined |
| Reduced volume and mass of final multifunctional subsystem |

the same piece of hardware (Type I Multifunctionality); electronics and thermal hardware are spread on the panel surface, eliminating the need for bulky apparatus and reducing size and mass with the co-location of different functionalities on the same spots (Type II Multifunctionality); materials are modified at millimiter scale: composites are tailored for optimal thermal and structural performance, while PCBs embed circuitry and thermal hardware in the same extremely limited volume.

## 4.2 STEPS Smart Skin

### Thermal Vacuum Test

At the end of the instrumentation process, before the beginning of the thermal vacuum test, the SDB demonstrator failed. The failure was due to a fault in the DC/DC converter group, probably caused by a short circuit in the 5V section. Due to this failure, the SDB prototype was excluded from the TVT and subject to inspection. After thorough examination, the demonstrator was repaired and re-programmed. The smart skin on the recovered prototype is still fully functional and the demonstrator can be operated thanks to a by-pass of the damaged converter.

After SDB failure, for schedule constraints, the thermal vacuum test was performed only on the SDA demonstrator, as shown in Figure 3.54 and described in Table 3.33. Moreover, due to an early failure during the TVT, smart skin number 5 was excluded and the test was performed with the other three samples. Reasons behind the loss of communication with smart skin n.5 are still under investigation.

Regarding Case 1, refer to Figure 4.12 for an overview of the timeline and the

various steps. The graph shows the behaviour of average temperature on the upper and lower side of the panel.

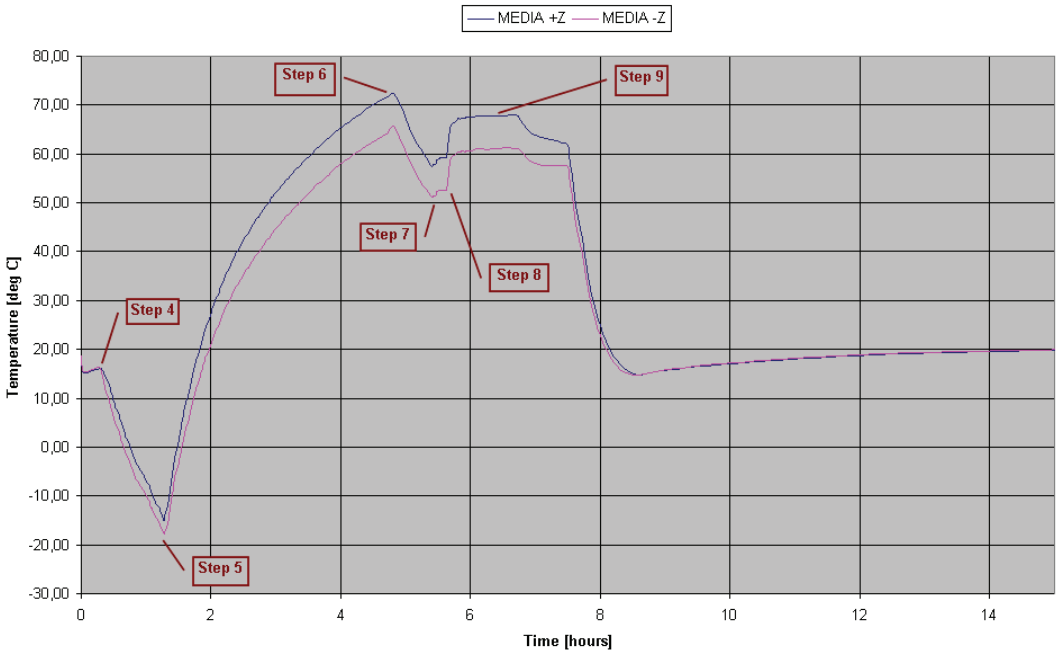


Figure 4.12: Case 1 - overview.

The scope of Case 1 was to validate design and COTS components for the smart skins, while showing its functionality at maximum operative temperature (70 °C). All the heaters onboard the smart skins were given a threshold command between 68 and 70 °C. With this approach, each heater is automatically activated when its reference sensor drops below the lower threshold and is turned off when the temperature grows over the maximum threshold (as reported, for example, in Figure 4.13 - heater A on smart skin 2)

A detailed record of +z temperatures during Case 1 is shown in Figure 4.14.

The numbering of thermocouples reported in graphs is compliant with Figure 3.43 and Figure 3.44. With respect to Figure 4.14, T7 is at higher temperature because it is mounted directly on H2. T1, T2 and T3 are at lower temperature because they are located near smart skin n. 5 which is not activated. T4 ÷ T6 and T8 ÷ T11 are near the reference set point (70°C). T12 and T13 are slightly colder than the other TCs because they are near the cable bundles, which cause a "gap" in the MLI insulation. Figure 4.15, Figure 4.16, and Figure 4.17 show the values recorded on the different temperature sensors for each smart skin at the end of Step 9. As can be easily seen, 13 out of 17 sensors are presented on the global user interface form. The other four sensors can be checked through the forms dedicated to different heaters (see, for example, Figure 4.18, Figure 4.19, Figure 4.20, and Figure 4.21 for smart skin 2).

Moving on to the next test phases, Figure 4.22 shows an overview of the timeline, the various cases (2, 3, and 4), and the various steps.

A detailed record of +z temperatures for Case 2 is shown in Figure 4.23.

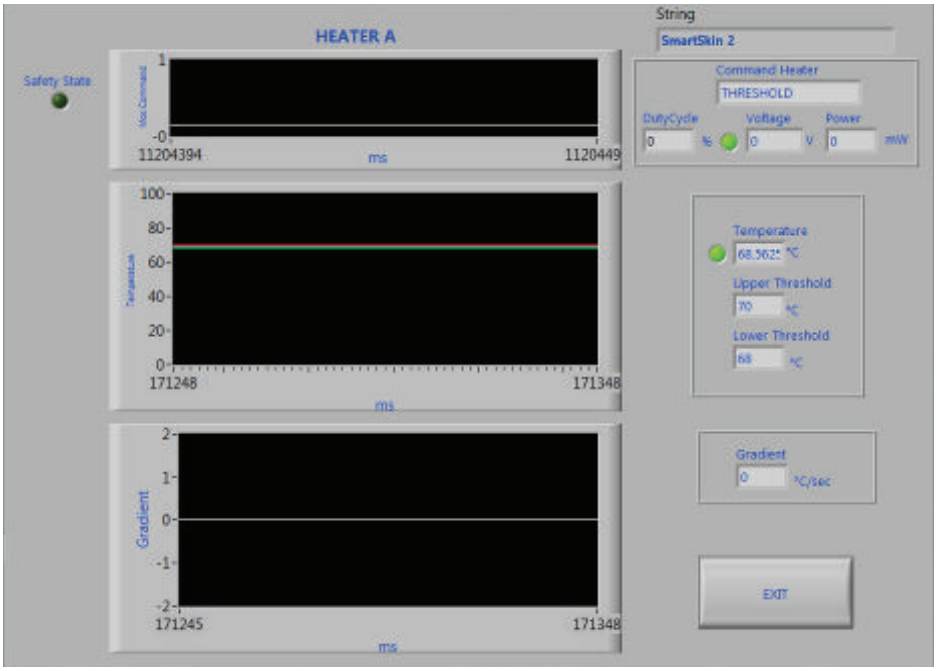


Figure 4.13: Case 1 - Heater A on smart skin 2 (dissipated power is 0 because the temperature is above the minimum threshold).

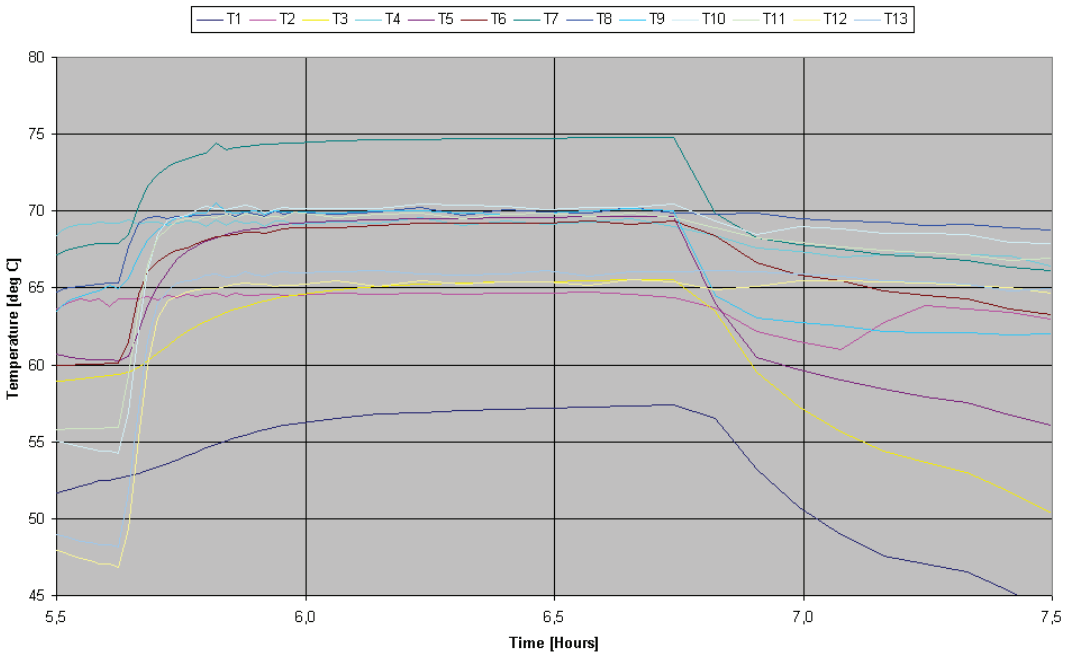


Figure 4.14: Case 1 - detail of +z temperatures during step 9.

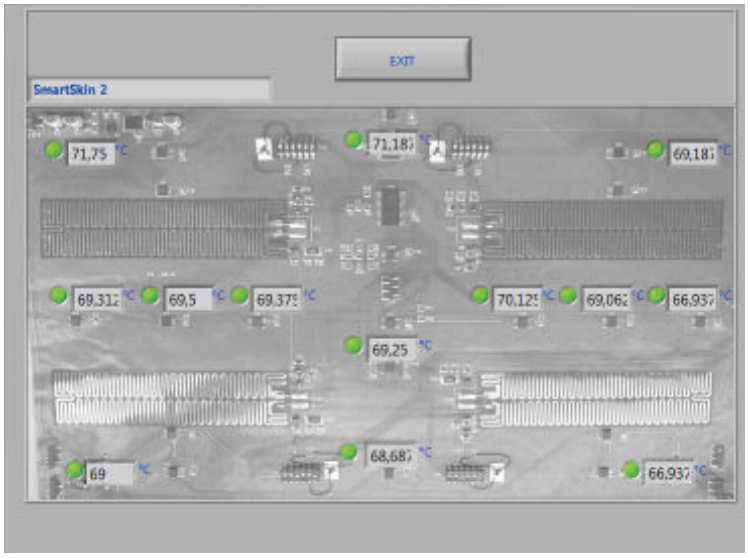


Figure 4.15: Smart skin n. 2 at the end of Case 1.

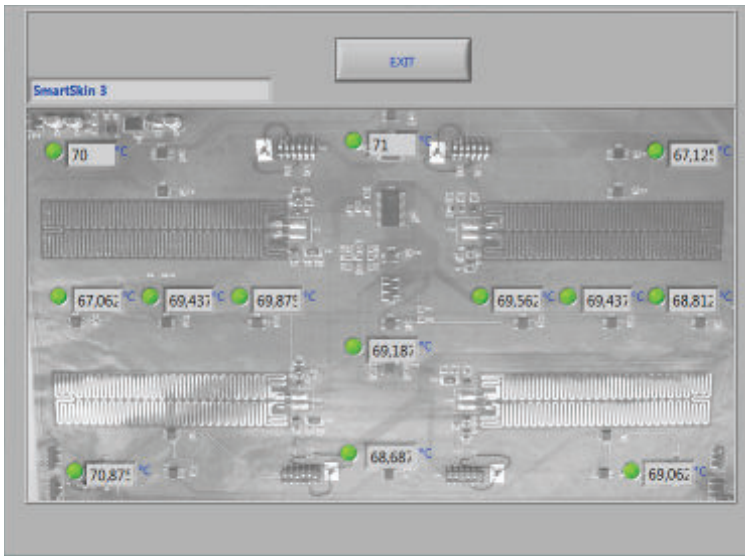


Figure 4.16: Smart skin n. 3 at the end of Case 1.

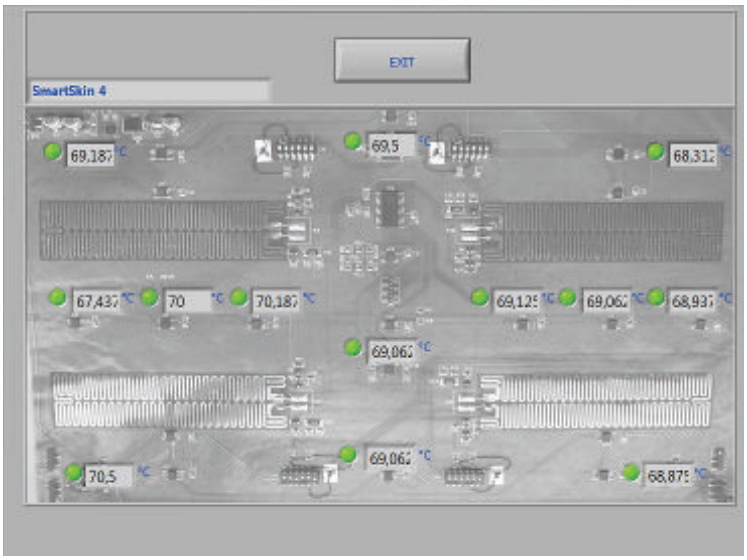


Figure 4.17: Smart skin n. 4 at the end of Case 1.


Figure 4.18: Smart skin 2, heater A at the end of Case 1.


Figure 4.19: Smart skin 2, heater B at the end of Case 1.


Figure 4.20: Smart skin 2, heater C at the end of Case 1.


Figure 4.21: Smart skin 2, heater D at the end of Case 1.

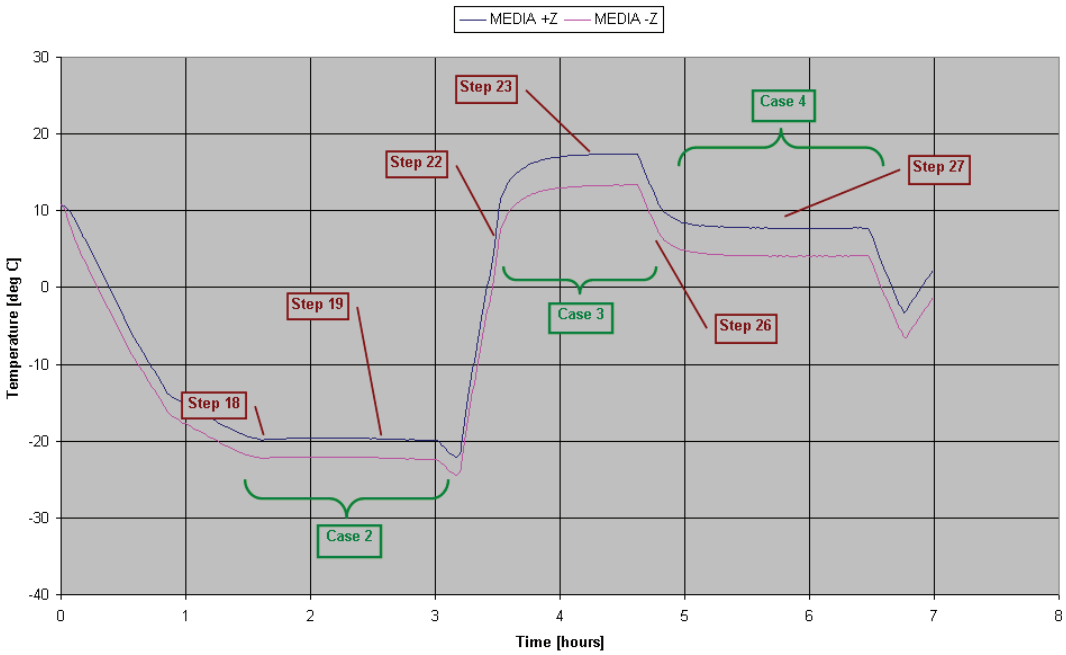


Figure 4.22: Cases 2, 3, and 4 - overview.

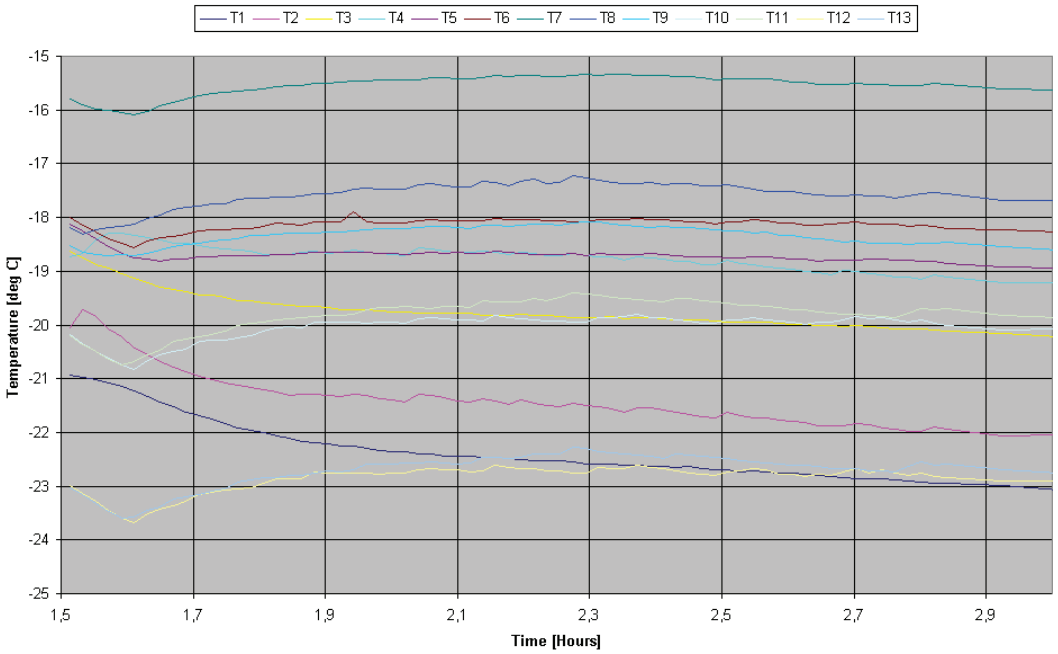


Figure 4.23: Case 2 - detail of +z temperatures during step 19.

The goal of this Case was to keep the motherboards functioning at their lower operative temperature (-20 °C). There was a software bug in the acquisition of the digital temperature sensors. The readout was correct for positive temperature, but for negative temperatures it showed an offset of +256 degrees centigrade (e.g., at 0+ °C the reading was 0 °C; at 0- °C the reading was +256 °C; at -1 °C the reading was +255 °C; at -20 oC the reading was +236 °C; and so on and so forth). Because of this bug, it was not possible to set a negative threshold. In this case a duty cycle command was instead applied. All heaters were given the target value of 5% duty cycle. For this reason, the temperatures shown in Figure 4.23 are less clustered around the target value with respect to those presented for Case 1.

A detailed record of +z temperatures during Case 3 is shown in Figure 4.25.

During this Case, all dummy units were turned on and all heaters were set to a threshold command between 19 and 20 °C. Thermocouples T1, T3, T6, and T5 are sensibly colder because they are placed near smart skin n.5, which is not activated. Moreover, TCs T2, T9, T12, and T13 are slightly colder than the set point because they are placed further from the heating devices (and, concerning T12 and T13, they are near cable bundles). Signals T4, T7, T8, T10, and T11 adhere well to the pilot command. Figure 4.26, Figure 4.27, and Figure 4.28 present the status of smart skins at the end of Case 3. They show the temperature values reported by the digital sensors mounted on the various motherboards.

At the end of this Case, the four sensors not shown in the aforementioned pictures read as listed in Table 4.5.

When Figure 4.28 was taken, the reference temperature for heater D onboard smart skin 4 was less than 19 °C. For this reason, heater D was activated. Figure 4.29 shows the status of the relevant control form: note that the duty cycle is set to 100%.

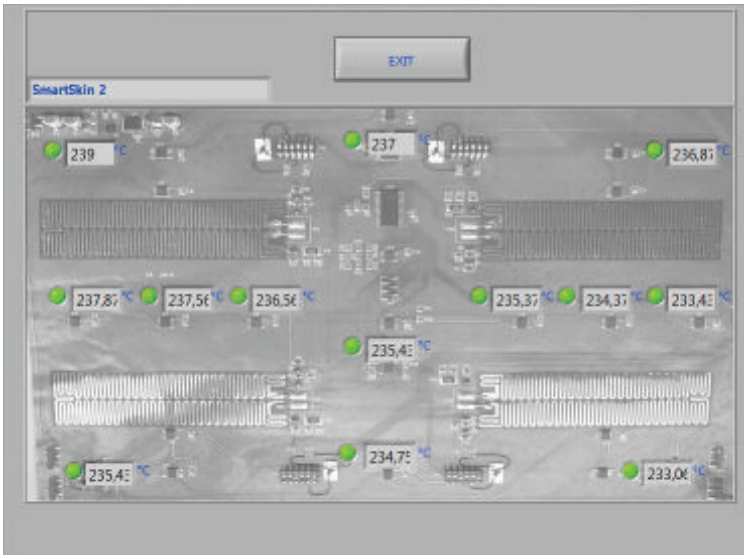


Figure 4.24: Temperature readings onboard smart skin 2 at the end of Case 2, showing software offset bug.

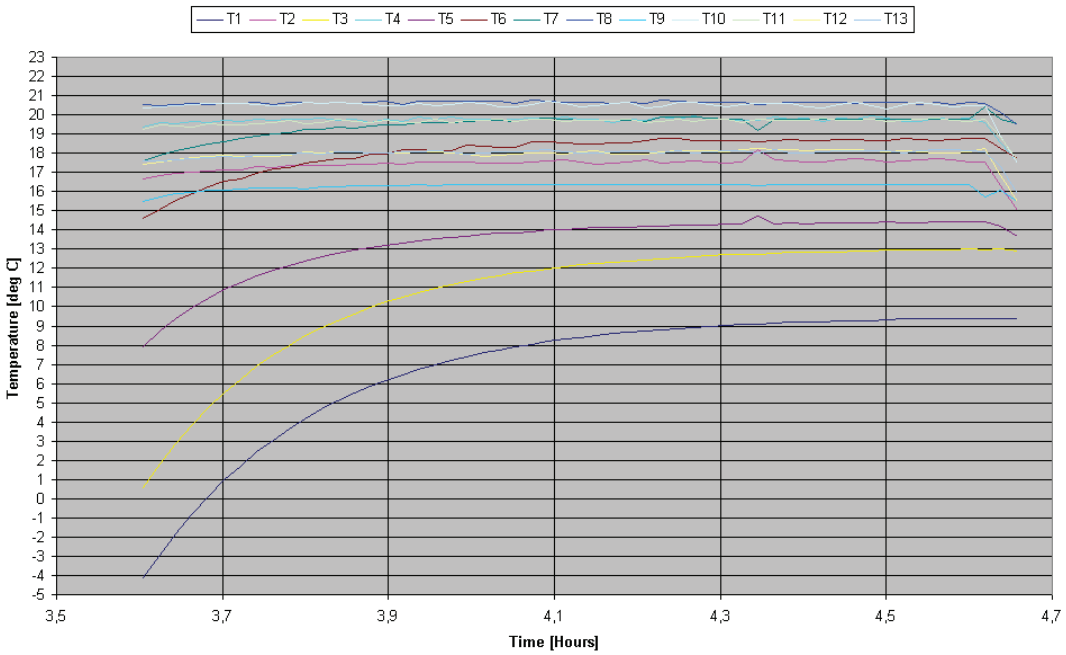


Figure 4.25: Case 3 - detail of +z temperatures during step 23.

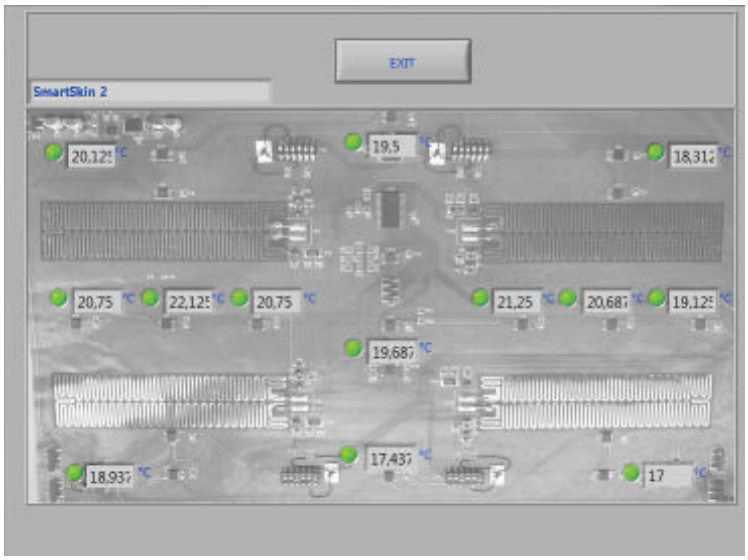


Figure 4.26: Smart skin n. 2 at the end of Case 3.

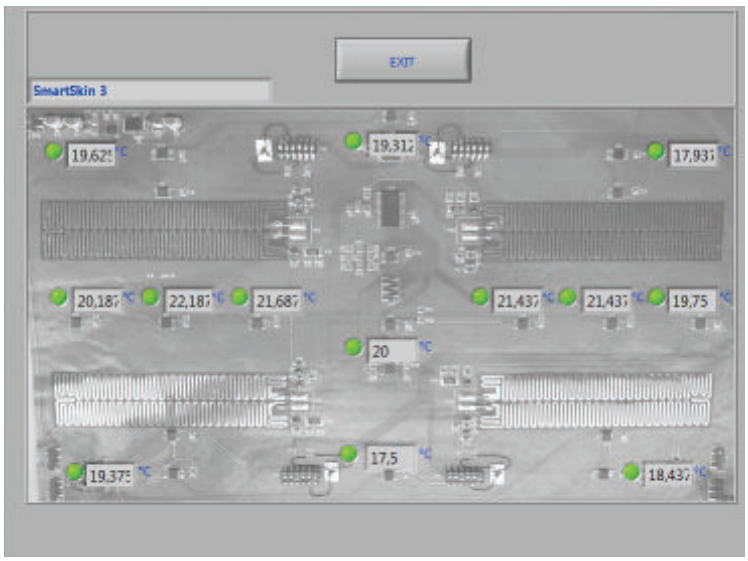


Figure 4.27: Smart skin n. 3 at the end of Case 3.

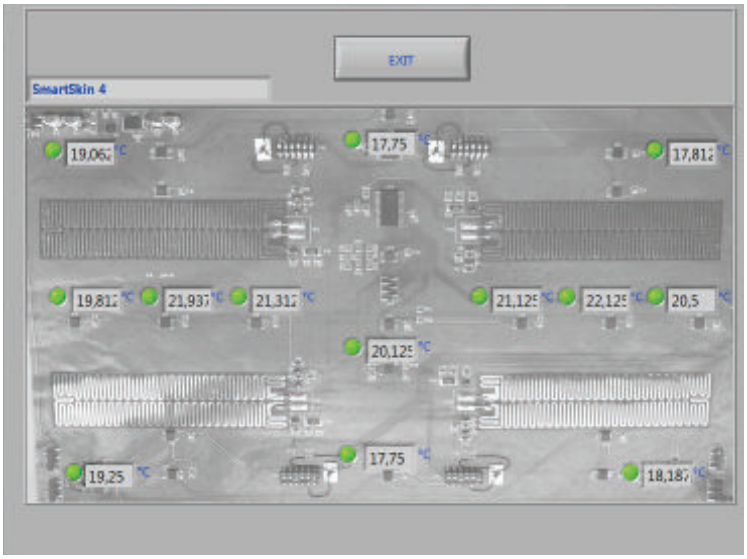


Figure 4.28: Smart skin n. 4 at the end of Case 3.

Table 4.5: Heater control temperature sensors at the end of Case 3.

| | |
|---|---|
| Smart skin 2 | HA = 20.06 °C |
| | HB = 20.81 °C |
| | HC = 19.31 °C |
| | HD = 19.25 °C |
| Smart skin 3 | HA = 21.31 °C |
| | HB = 20.94 °C |
| | HC = 19.13 °C |
| | HD = 19.00 °C |
| Smart skin 4 | HA = 20.63 °C |
| | HB = 19.00 °C |
| | HC = 19.44 °C |
| | HD = 18.94 °C |

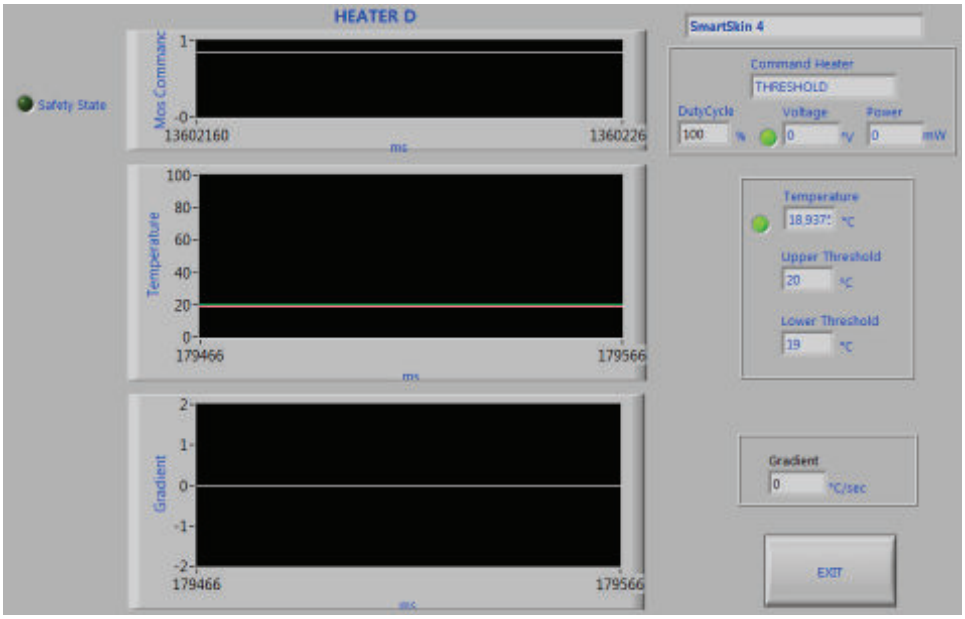


Figure 4.29: Heater D onboard smart skin n. 4 at the end of Case 3.

During Case 4, all heaters were instructed to keep the motherboards between 9 and 10 °C. This was done, as usual, with the threshold command. A detailed record of +z temperatures regarding Case 4 is shown in Figure 4.30.

Signals T1, T3, and T5 are sensibly lower than the reference temperature because they are placed near smart skin n.5, which is not activated. Temperatures registered by TCs T2, T6, T9, T12, and T13 are slightly colder than the set point because these sensors are placed further from the heating devices (and, concerning T12 and T13, they are near cable bundles). Thermocouples T4, T7, T8, T10, and T11 show values which adhere well to the pilot command.

Proceeding with the thermal vacuum test, Figure 4.34 shows an overview of the timeline, and the various steps of Case 5. The goal of Case 5 was twofold: first of all, to prove the functionality of the power command to smart skin heaters (step 37), secondly, to operate once again the motherboards at their maximum operative temperature (step 40).

A detailed record of +z temperatures regarding Case 5 is shown in Figure 4.35. Signals T1, T3, T5 are sensibly lower than the reference temperature because they are located near smart skin n.5, which is not active. Temperatures registered by TCs T2, T6, T9, T12, and T13 are slightly colder than the set point because they are placed far from heating devices (and, concerning T12 and T13, they are near cable bundles). Thermocouples T4, T7, T8, T10, and T11 show values which adhere well to the pilot command.

### Ambient Test

Looking at data collected during ambient testing, Test Phase 1 confirmed the coherence of data collected through digital sensors with data collected through thermocouples. Figure 4.39 and Figure 59 are given for reference. Room conditions were Pamb = 1007 mbar and Tamb = 23.3 °C. Data from Channel 1 and Channel

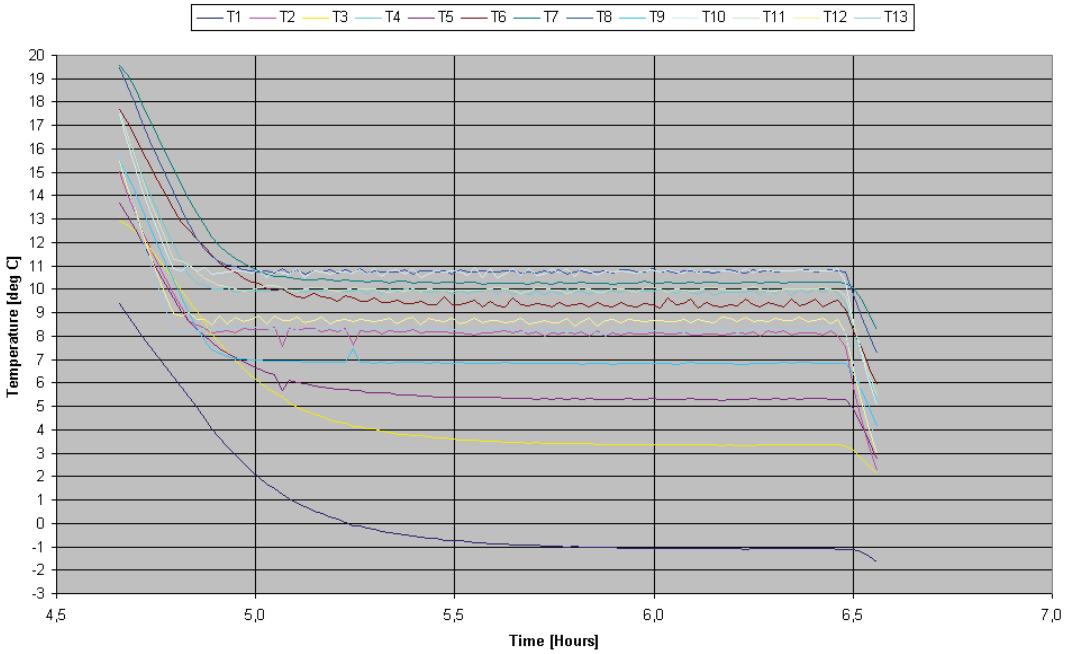


Figure 4.30: Case 4 - detail of +z temperatures during step 27.

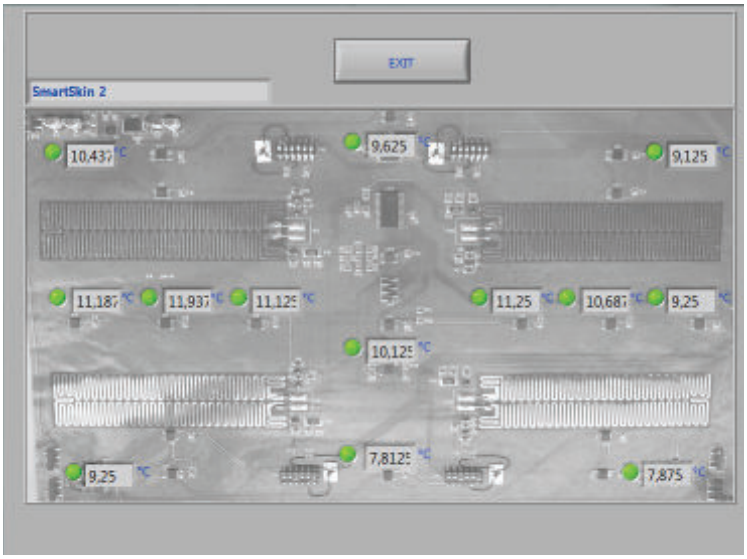


Figure 4.31: Smart skin n. 2 at the end of Case 4.

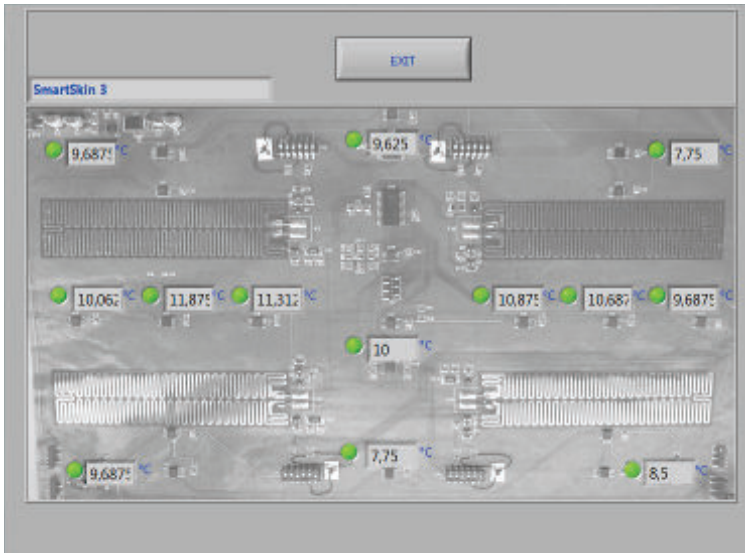


Figure 4.32: Smart skin n. 3 at the end of Case 4.

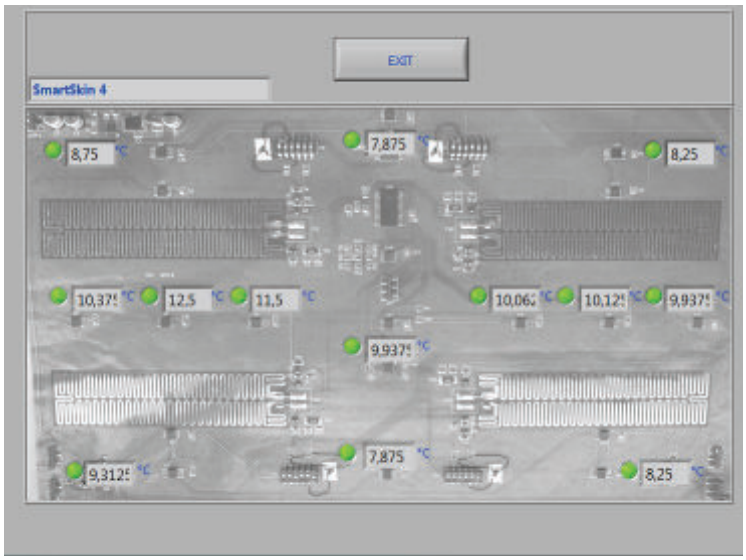


Figure 4.33: Smart skin n. 4 at the end of Case 4.

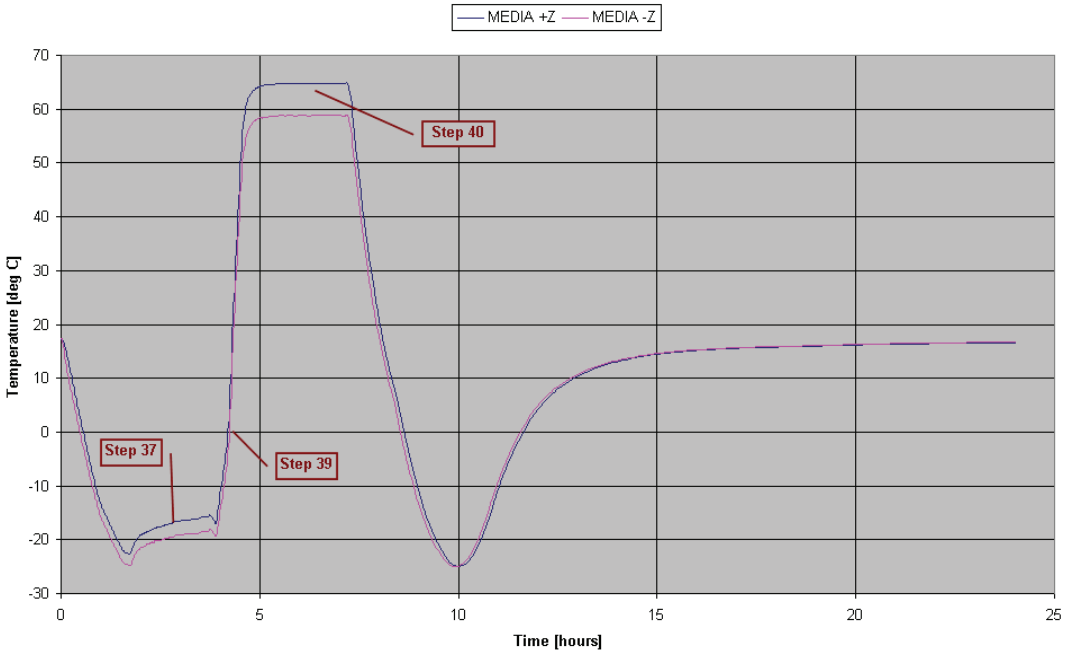


Figure 4.34: Case 5 - overview.

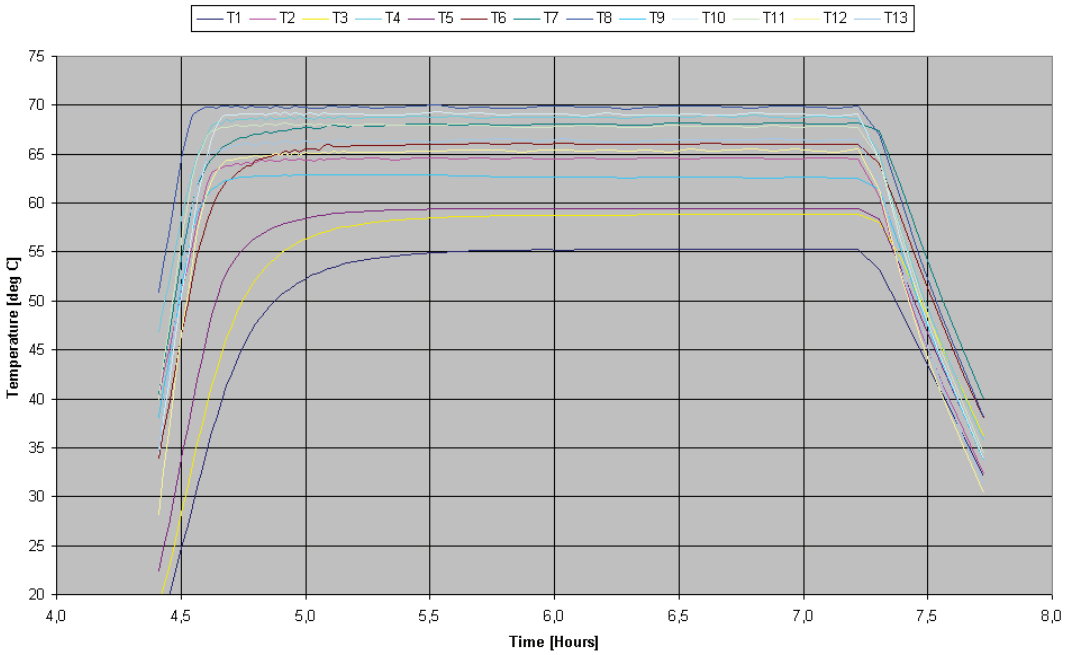


Figure 4.35: Case 5 - detail of +z temperatures during step 40.

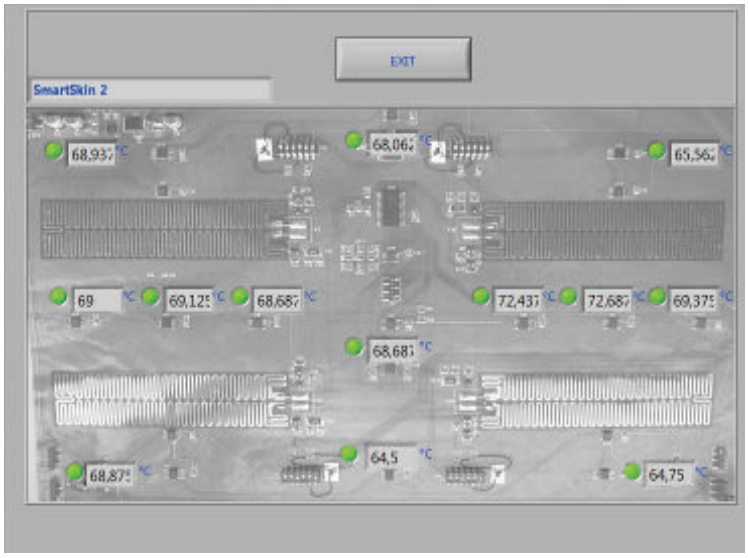


Figure 4.36: Smart skin n. 2 at the end of Case 5.

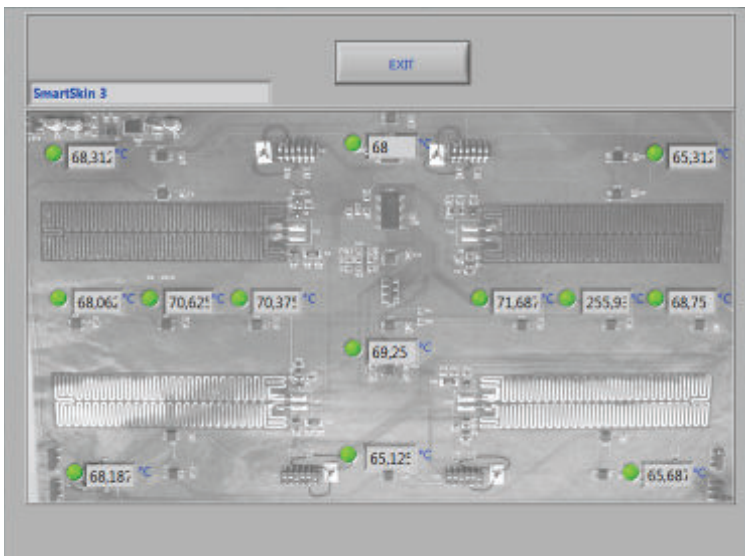


Figure 4.37: Smart skin n. 3 at the end of Case 5.

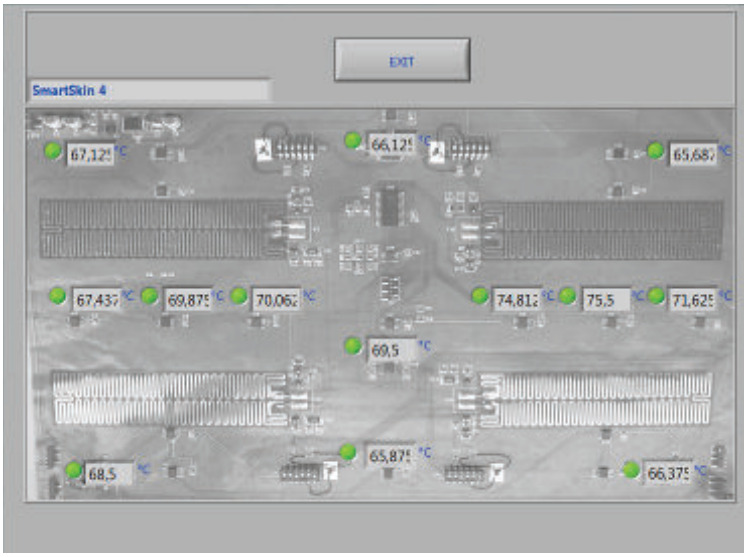


Figure 4.38: Smart skin n. 4 at the end of Case 5.

5 are higher than the other ones because these two thermocouples were placed near the DC/DC converter and therefore they sensed its activity. For a similar reason, the temperature recorded by Channel 3 was slightly higher than the value read on U32 (the microcontroller and the I/O expander dissipate heat while the smart skin is working). These behaviors are found in all test phases. Referring to the scope of Phase 1, it is proven that there is good correspondence between thermocouples and digital sensors.

Test Phase 2 starts with the following ambient conditions: Pamb = 998 mbar and Tamb = 20.3 °C. The goal is to verify the performance of the threshold command control law. To apply this control methodology, it is necessary to set two input parameters: the minimum and the maximum allowed values for heater's temperature. The threshold law belongs to the ON÷OFF kind of control, therefore the function output is a pulse width modulation (PWM) with:

- 100% duty cycle (ON status) when the reference temperature drops below the minimum threshold.
- 0% duty cycle (OFF status) when the reference temperature rises over the maximum threshold.

In Phase 2, the lower threshold was set equal to 24°C, while the upper threshold was set equal to 26°C. Results obtained from the SDC test are shown in Figure 4.42 and Figure 4.43. The heating and cooling cycles due to the ON÷OFF strategy are clearly visible. As explained in the previous section, Channel 1 and Channel 5 are sensibly warmer than the other control points because they are placed near the DC/DC converter. It is also good to notice that, being an ambient test, the convective heat exchange with the surrounding atmosphere is responsible for the greater outflow, while the in-plane heat distribution is attenuated by the low thermal conductivity typical of polyimides and aramids. With all considered, the performance of the threshold control law is satisfactory.

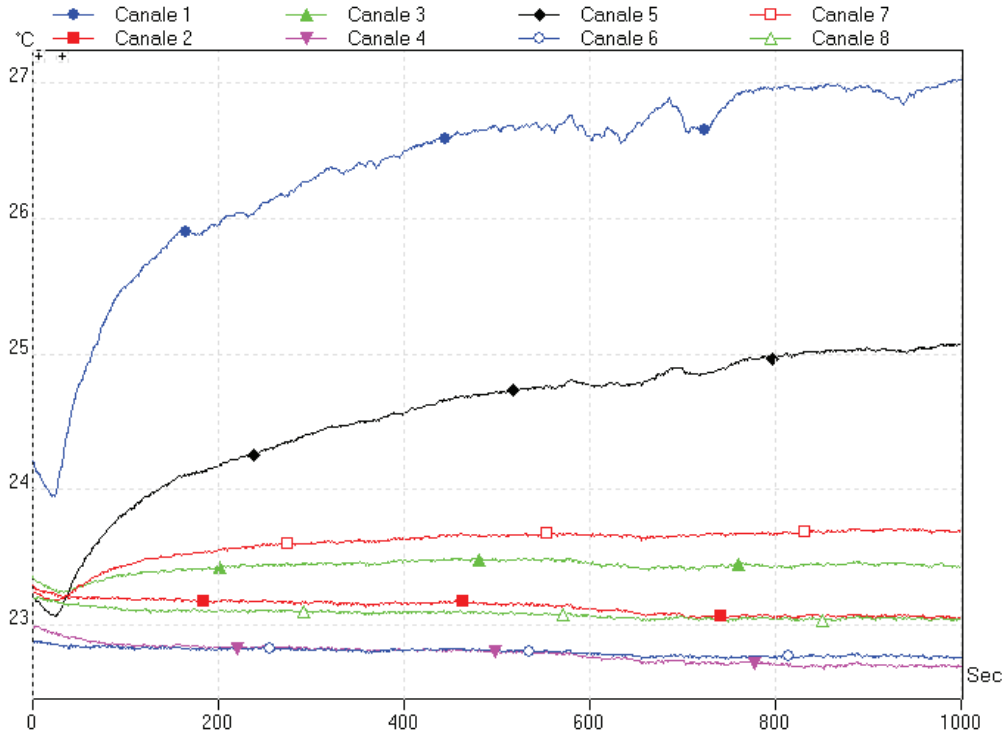


Figure 4.39: Phase 1 - Data obtained with TCs.

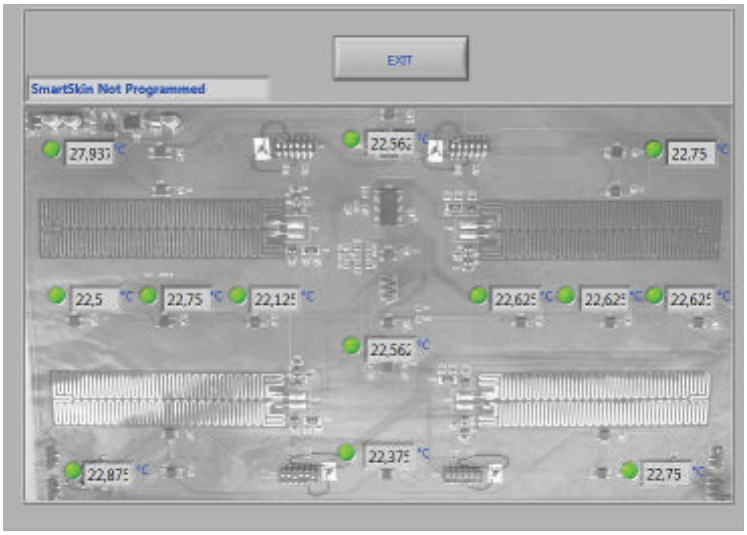


Figure 4.40: Phase 1 - Data obtained with smart skin's sensors.


Figure 4.41: Phase 2 - Command sent to the smart skin.

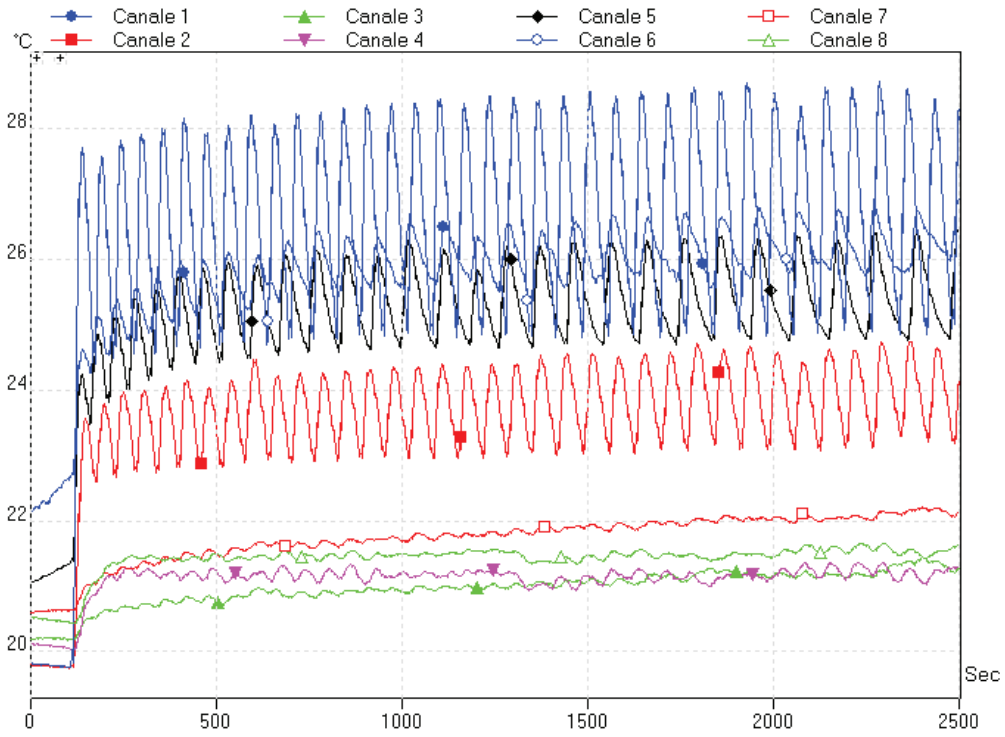


Figure 4.42: Temperatures measured during Phase 2.

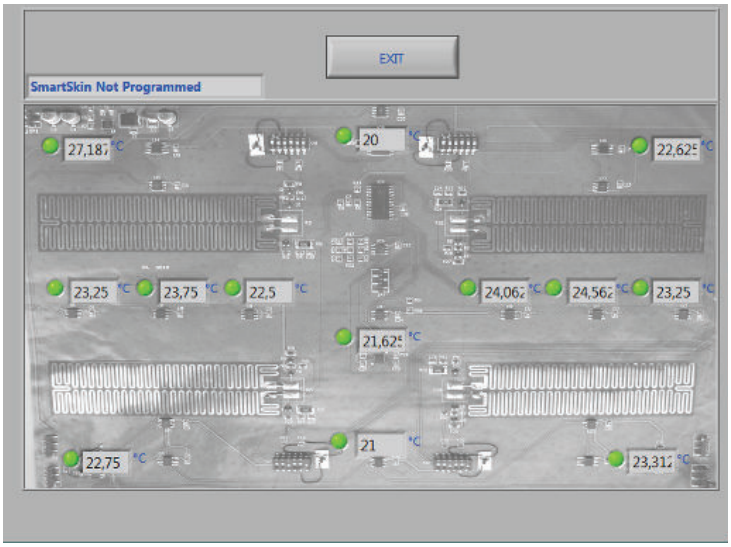


Figure 4.43: Temperatures measured onboard the smart skin at the end of Phase 2.

Test Phase 3 was carried out to check the performance of the power target control law. The PWM is computed according to the input parameter, and there is not direct feedback from heater's temperature.

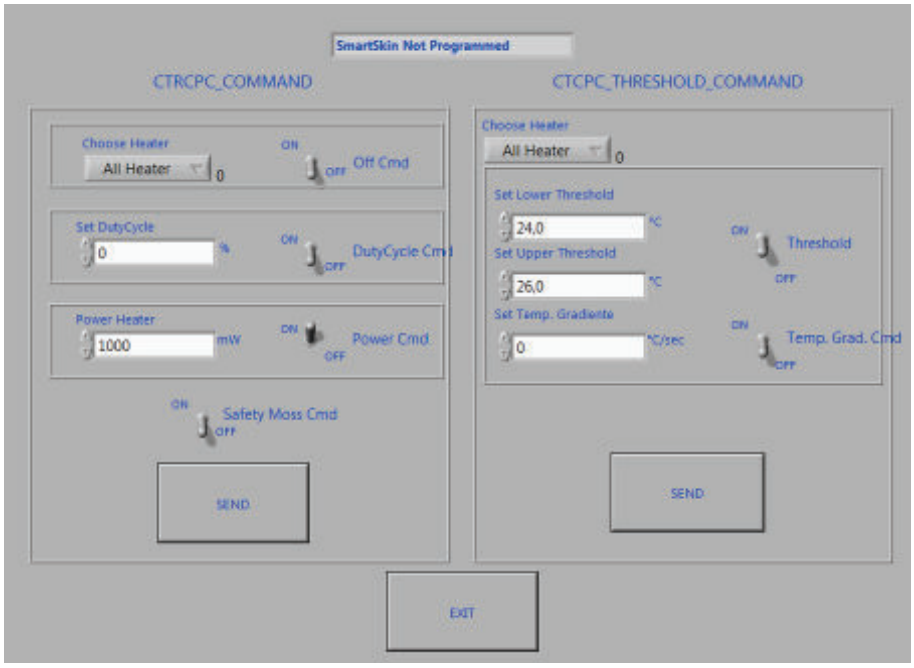


Figure 4.44: Phase 3 - Command sent to the smart skin.

Results for Phase 3 are shown in Figure 4.45 and Figure 4.46.

The initial spike that can be seen in Figure 4.46 is just a negligible transient between Phase 2 and Phase 3. During the descending front, the power command was activated, applying 1 W to each heater. That moment corresponds to a sudden change in graph slope, and temperatures start rising again. Since the feed voltage varies slightly, the supplied power (PWM) is constantly adjusted, and this causes

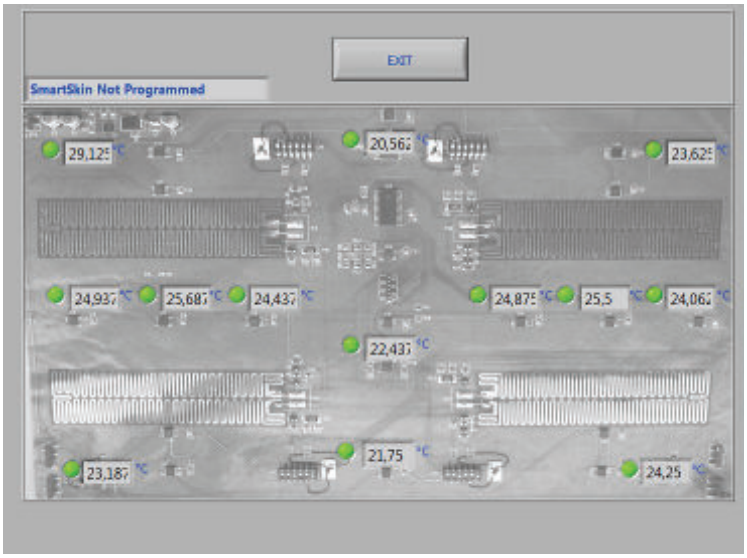


Figure 4.45: Temperatures measured by the digital sensors at the end of Phase 3.


Figure 4.46: Temperatures recorded during Phase 3.

visible fluctuations in the recorded temperatures. Since each heater has a maximum rating of 9 W, and since the average target value of 1 W is obtained with a variable duty cycle (and not with a variable voltage or current), there are instantaneous peaks where the smart skin absorbs ∼36 W (28 V, 1340 mA): these peaks correspond to moments where all four heaters are contemporaneously ON. Generally speaking, the control law behaves correctly.

Test Phase 4 was started at Pamb = 996 mbar, and Tamb = 21.6 °C. The scope was to check the performance of the gradient target control law. Here gradient means time derivative. There are three input parameters: the temperature delta in the given time step (°C/s), a maximum temperature and a minimum temperature. Similarly to what is done by the threshold control law, the temperature will be kept between the two limit values, but in this specific case, instead of using a simple ON ÷ OFF technique, the selected duty cycle is proportional to the selected rate of change of the reference temperature. Empirical tests show that the rate of change depends on initial conditions and external loads; at higher temperatures the variation of temperature in time is not linear.

During this phase, the gradient command control law was working, but its performance was not completely satisfactory. In fact, the algorithm has some flaws and only works well in a small neighborhood of the initial temperature, where the time evolution of T can be approximated with a straight line. After a few seconds, the real behaviour deviates from the linear approximation and shows clearly its tendency to reach a steady state value (plateau). Moreover, it is not possible to dictate a rate of change lower than unity (1 °C/s).

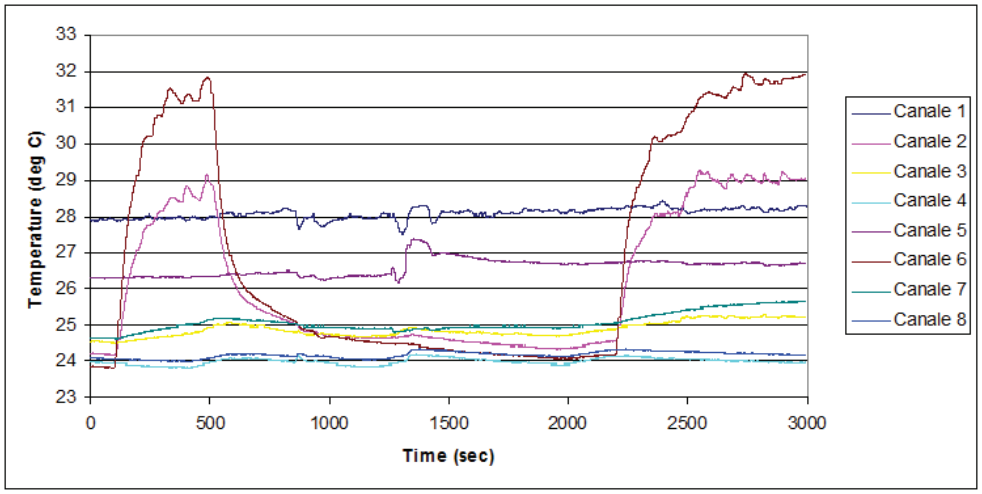


Figure 4.47: Temperatures measured during Phase 4.

Figure 4.47 shows the behaviour of the gradient target law. At t=100 s heater C was turned on with the following parameters: upper threshold equal to 46 °C, lower threshold equal to 44 °C, and gradient equal to 10 °C/s. The response of the system was to turn on heater C at 17÷18% duty cycle, therefore dissipating 1470÷1550 mW, and showing an initial increase of 0.1 °C/s. Then the increase slowed down and met a series of plateaus in the range 30÷32 °C. The heater was manually turned off at t=500 s, and the smart skin was left to cool down to the

initial condition. As a verification, after the system reached the same temperature that it had at the beginning of the phase (t=2200 s), heater C was turned on via the duty cycle command:

- At first it was assigned a 17% duty cycle (corresponding to ∼1460 mW of dissipated heat).
- Then it was turned on at 18% duty cycle (∼1550 mW).

The response of the system to this second load was very similar to the first part of Phase 4, and subsequently we can state that this control law needs specific improvement, in order to allow a better control of the temperature gradient.

Test Phase 5 was devoted to checking the performance of the duty cycle command control law. In this case, the user has direct control over the duty cycle and can set it to a desired value. The reference temperature is not controlled, and therefore the same considerations made for the power target law apply.

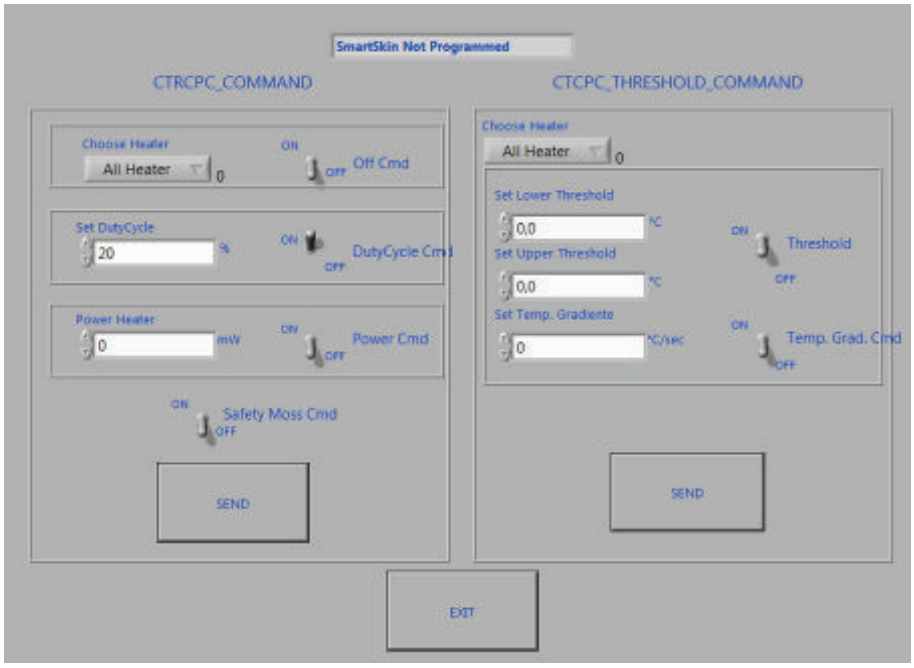


Figure 4.48: Phase 5 - Command sent to the smart skin.

Results are shown in Figure 4.49 and in Figure 4.50. The control law behaved as foreseen. There are small fluctuations due to the PWM regulation, but the temperature clearly tends to a steady state condition depending upon the required duty cycle (which implies a certain power dissipation).

Test Phase 6 requires heating SDC up to the maximum operative temperature, i.e. 70 °C. Of course this is a limit case, since a smart skin installed inside a manned inflatable structure will presumably be bounded to operate below 40 °C, for crew safety reasons. Nonetheless, it is useful to verify the behaviour of the assembly at higher temperatures, in order to check its sensitivity to temperature spikes and understand if hot spots can damage the flexible motherboards or reveal fabrication

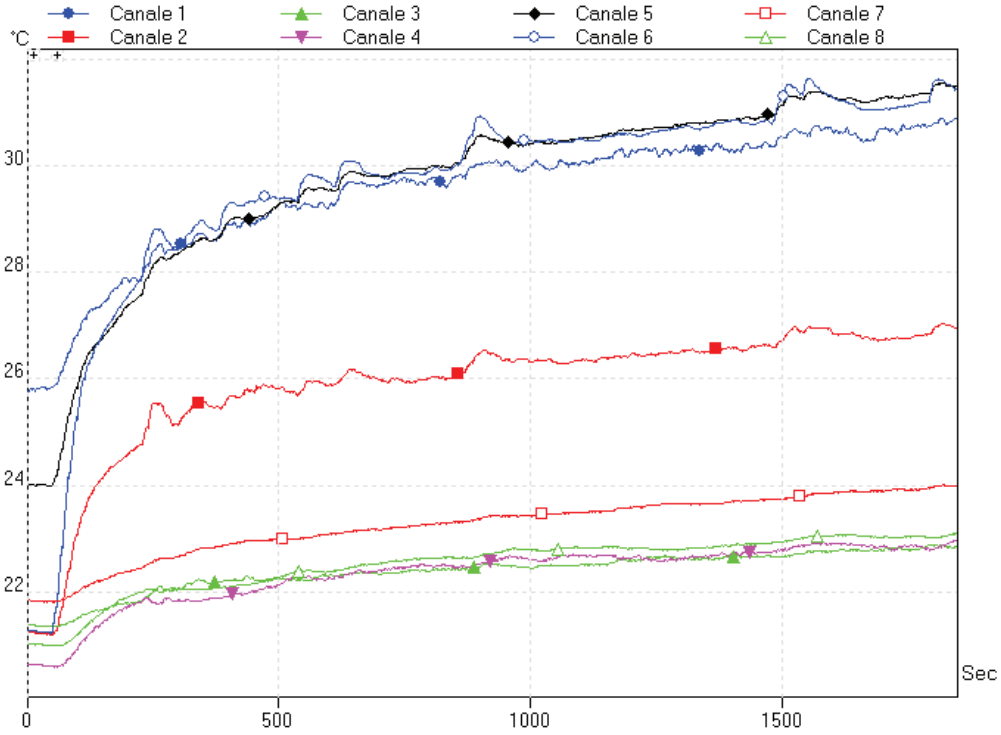


Figure 4.49: Temperatures measured at the end of Phase 5.

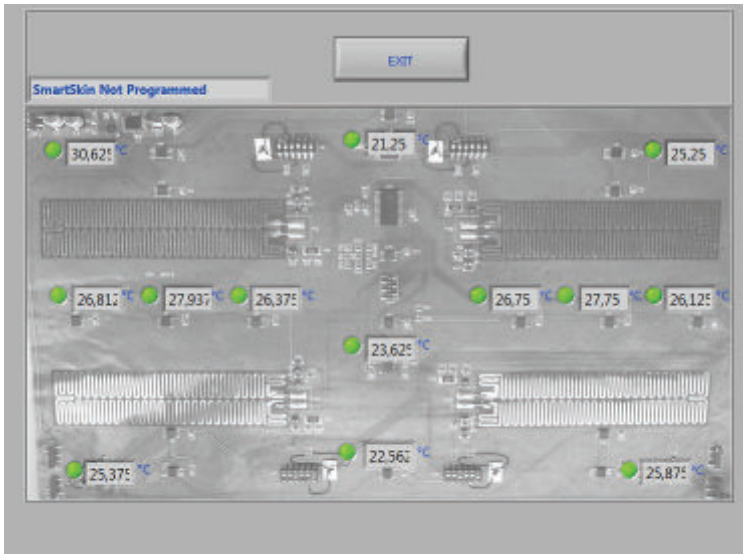


Figure 4.50: Temperatures measured by digital sensors at the end of Phase 5.

flaws (e.g. discontinuities in bondings). For convenience, the goal of keeping the smart skin at the desired temperature was achieved through the threshold control law.

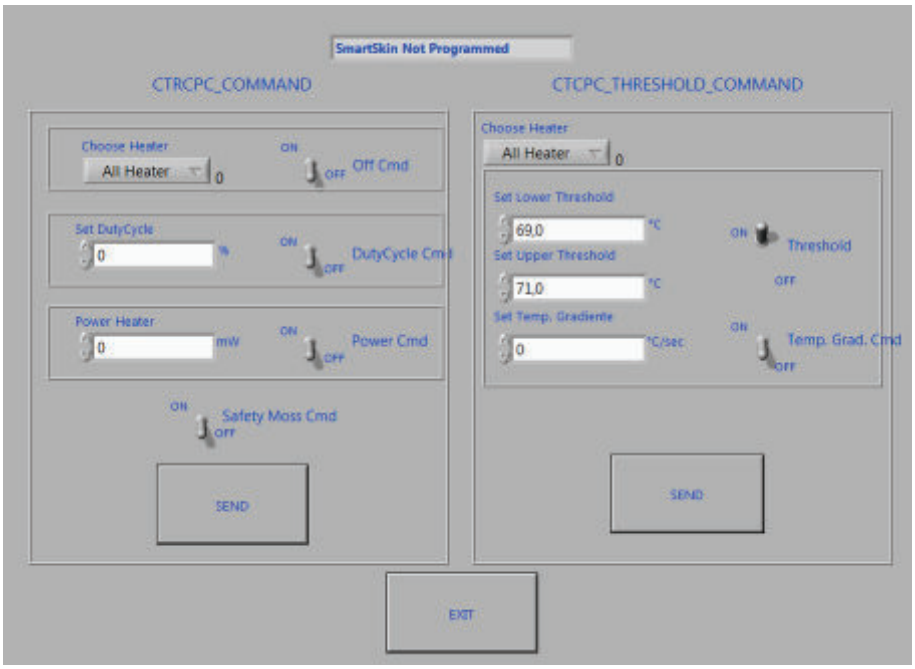


Figure 4.51: Phase 6 - Command sent to the smart skin.

Results referring to Phase 6 are depicted in Figure 4.52 and Figure 4.53. At the end of this phase, all reference temperatures for the four heaters are between 69 and 71 °C. Of course, given the low in-plane thermal conductivity of the smart skin and its support, and given the high convective heat exchange, the temperature in points far from heaters is sensibly lower than 70°C. The power consumption is ∼36 W (28 V, 1330 mA), showing that all heaters are ON at maximum dissipation.

While in this configuration, some air bubbles appeared under the heaters, revealing that some gas was trapped during the gluing process. However, no dangerous detachment was detected. All heaters continued to perform correctly and there was no disjoining of the smart skin from the support fabric.

The last test phase, Phase 7, was carried out in order to verify the performance of the smart skin while subject to vibrations and to sensible flexure. The smart skin was kept between 24 and 26 °C via a threshold command (see Figure 4.54).

At first, small shocks (∼2 g) in the two planar directions (x and y) were applied while reading the temperature sensors and checking accelerometer data. No interruptions of CAN traffic or anomalies in temperature data were detected: the smart skin continued to perform correctly. The accelerometer signalled correctly the movements; even if a small noise was always present (∼0.4 g in both directions). Then the smart skin was flexed and shaken gently, while monitoring the bus behaviour: there was no problem with data communication. Finally, the motherboard was bent with a radius of ∼40 mm around the x axis (refer to Figure 75) and kept in place working for 15 minutes. There was no kind of problem or degradation of the smart skin performance.

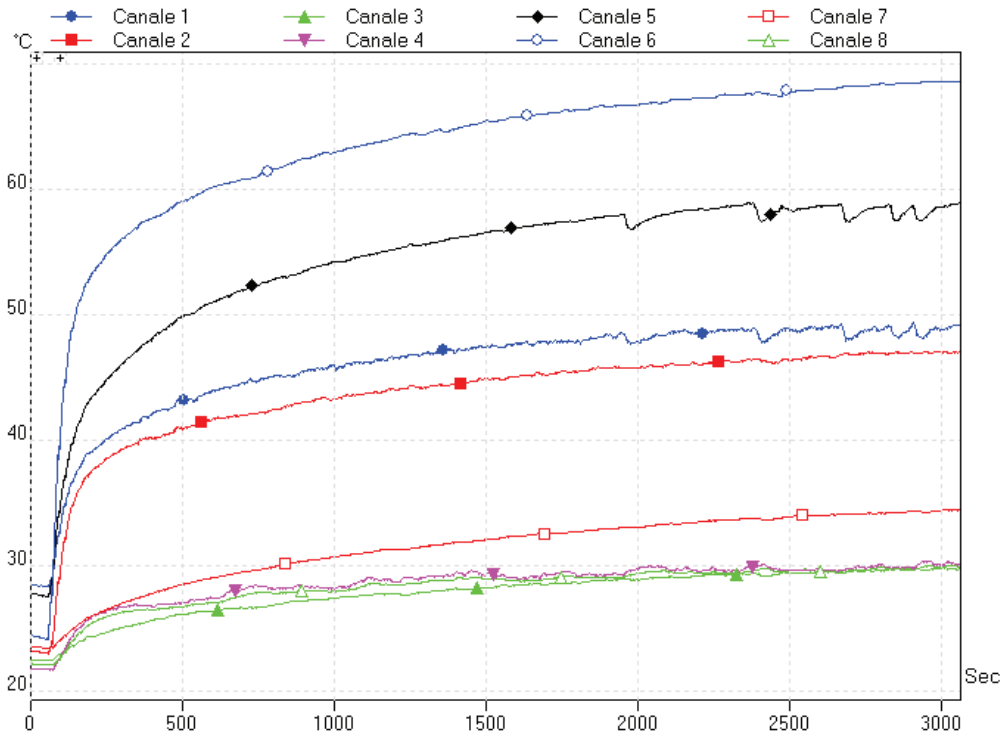


Figure 4.52: Temperature log for Phase 6.

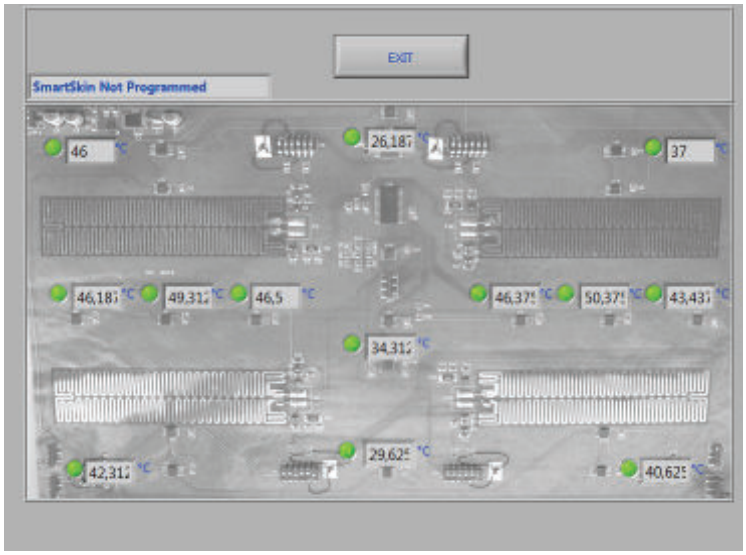


Figure 4.53: Temperatures shown by smart skin's HMI at the end of Phase 6.


Figure 4.54: Phase 7 - Command given to the smart skin.

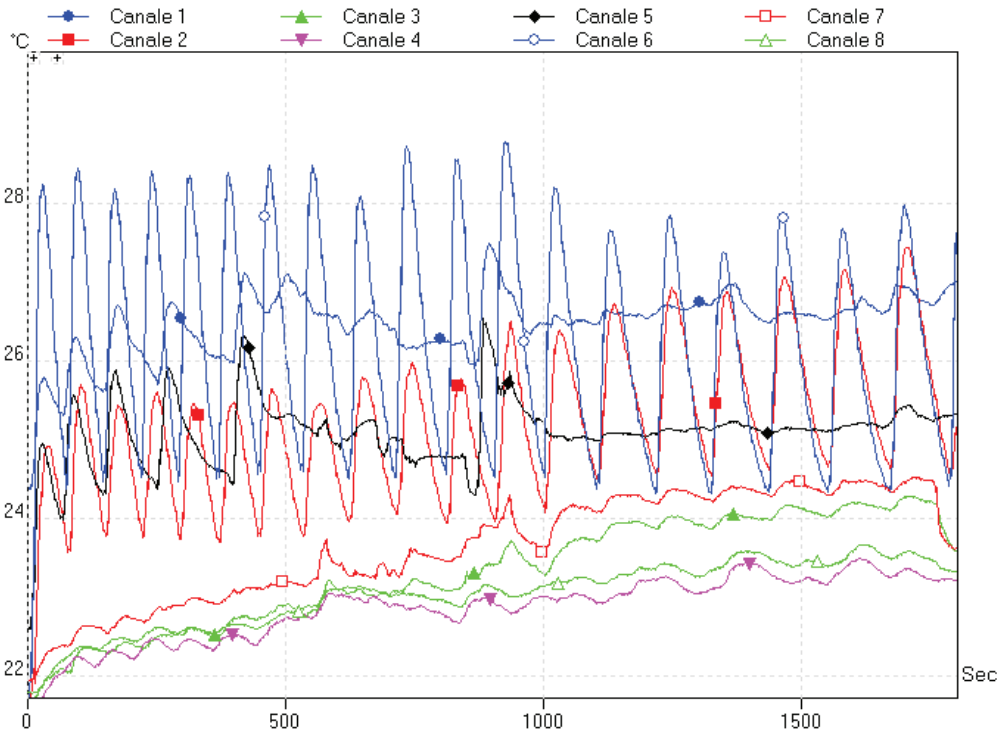


Figure 4.55: Log of TCs during Phase 7.

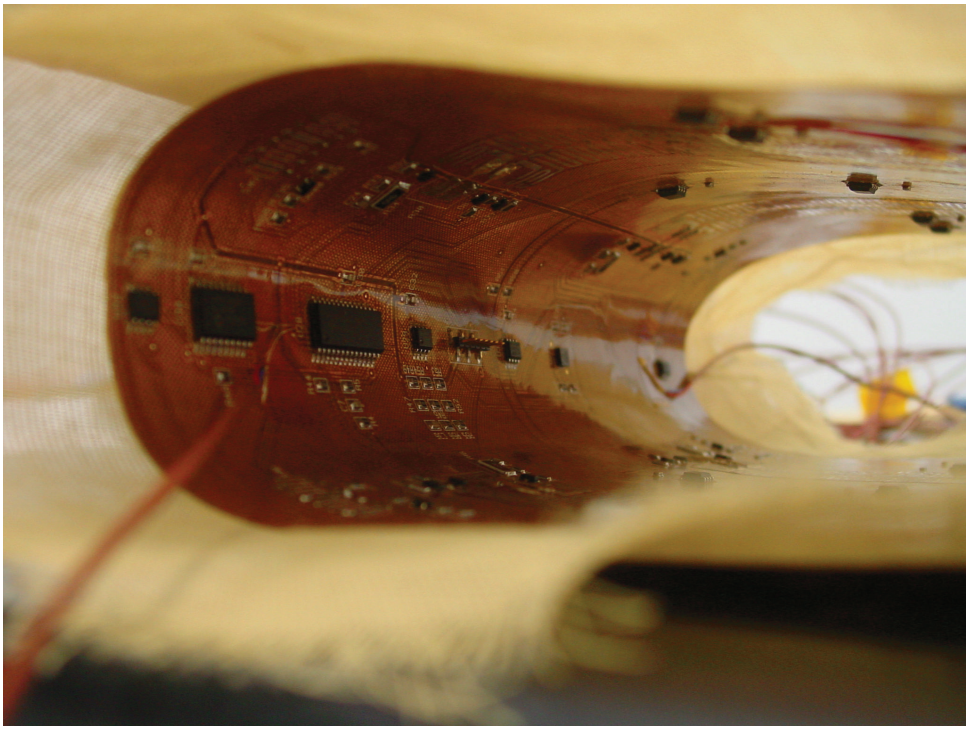

Figure 4.56: SDC bent with a 40 mm radius.

The STEPS smart skin demonstrators incorporate all the guidelines to obtain a migration from rigid electronic structures to new electronic conformal design in space applications. The demonstrators confirm that several features of the concept are valid, including design methods, elimination of chassis and cabling bundles, use of flex circuitry in novel ways with functional routing of signals and power, inclusion of monitoring and actuation in a single layer, assembly, integration and test procedures. A viable intermediate solution for the integration of heating function in the motherboard is the inclusion of flexible foil heaters tailored by the manufacturer for seamless inclusion in the smart skin. Up to now, the maximum motherboard size that is compatible with machines and processes is 420 mm x 300 mm. Keeping in mind standard panel sizes and maximum dimensions allowed by the vendors' machines is a good way to keep costs under control and avoid custom work. The number of conductive and insulating layers that can be stacked together depends on electrical and mechanical constraints like flexibility, presence of ground planes... but in general two to four conductor layers are compatible with the smart skin approach. In fact, adhesiveless flex that is etched on both sides is amazingly flexible: a sample can be hard creased up to seventeen times without breaking a trace, and if a 3 mm bend radius is used, one can easily attain one million flex cycles without failures[3]. At higher layer counts, the printed circuit board gradually loses flexibility and may need to have the bends added during the fabrication process, or, if the thick area is limited, it can be manufactured as a bookbinder. Today, a good number of specialized manufacturers have the capabilities to process this kind of multifunctional system, given the fact that the constitutive technologies are well

[3]This is the approach taken with laptop computer hinge joints that must carry the signals to the screen, or with cell phones and PDAs.

developed in the industry: in fact, many of these principles are already used in automotive applications.

After the early failure of the SDB demonstrator, for schedule constraints, the thermal vacuum test was performed only on the SDA prototype. Nonetheless there were enough samples to verify the behavior of COTS electronics in the thermal-vacuum environment. All the components survived the space-representative conditions with no degradation in their performance, they worked smoothly for extended periods both at their maximum and at their minimum operating levels. The digital temperature sensors showed a good matching with thermocouples' readings.

The motherboards were glued to their panels with Hysol®EA9321, a two-component epoxy paste adhesive qualified for space usage, and often applied as potting and structural repair medium in aerospace Maintenance Repair and Overhaul (MRO) activities. This thixotropic adhesive was chosen because it is suitable for room temperature cure, and it has good elevated temperature strength (it still retains 6.9 MPa ASTM D1002 Tensile Lap Shear Strength at 120 °C.). Part A and Part B components have densities equal to 1.24 and 1.22 g/ml respectively, and, after being mixed with a weight ratio of 100:50, they yield a mix with 1.23 g/ml density and a pot life of 40 minutes. Volume measurement is not recommended for structural applications, unless special precautions are taken to assure proper ratios. Bonding surfaces should be clean, dry and properly prepared. Therefore, the support structures have been degreased with isopropyl alcohol, then the motherboards' shapes have been transferred on the skins, and masked with Teflon tape. The adhesive has been mixed and applied with a spatula. Then the mask has been removed, and the motherboards have been placed. The result has been checked for smearing and defects, with particular care to the elimination of any gaseous bubble potentially trapped under the polymeric sheets. Then the bonded parts have been held in contact by means of vacuum bagging until the adhesive was set. Since handling strength for this adhesive is reached in 24 hours at room temperature, the vacuum bag was removed after one day and the joints were let to cure at 25 °C for a week [4]. The joint had a CTE of 102 ppm/°C, TML = 1.06%, CVCM = 0%, and WVR = 0.35%.

The thermal vacuum test positively verified the mechanical behavior of the flexible PI/Cu circuitry and its bonding procedure. No damage or degradation were shown after thermal cycling and vacuum exposure.

The functionality of the complete smart skin network, at its intended size and configuration, has been tested in the TAS-I TS-ETA test area. No control or acquisition problem has been identified in scaling up the network.

The ambient test conducted on STEPS demonstrator C partially verified the possibility to use the smart skin or a similar multifunctional layer in deployable or inflatable structures. The smart skin was bonded to a Kevlar cloth using a space qualified bi-adhesive tape: 3M Y966. Y966 is a commercial acrylic transfer tape adhesive, with fairly good space heritage. It is 2.0 mil thick, recommended for flexible circuits attachment, and for use in high temperatures. It is usable for short periods (minutes, hours) at temperatures up to 230°C and for longer periods (days,

[4]The adhesive cures at room temperature in 5÷7 days, or at 82 °C in 1 hour.

weeks) up to 150°C. Its bond strength generally increases after thermal cycling and ageing. Once properly applied at temperatures between 20°C and 38°C, it is tolerant to low temperatures (down to -40°C), even if tests for shock service are recommended. The final joint has TML = 0.93%, and CVCM = 0.01%, thermal conductivity of 0.18 W/m/K, and CTE = $5.8{\cdot}10^{-4}$ mm/mm/°C.

The bonding process included: application of the adhesive to the clean motherboard, pressing in place with a pre-vacuum bag, removal of adhesive liner, application of the motherboard onto Kevlar fabric, and second vacuum bag treatment. In particular, the vacuum bagging has been deemed necessary since it was not possible to roll the surface completely, due to the presence of SMD components.

Having a spare prototype motherboard, an additional bonding process to Kevlar cloth has been tried using a quite similar product by 3M: VHB®9460PC Adhesive Transfer Tape, a very firm 2.0 mil thick acrylic pressure-sensitive system, with very high shear holding power, and bond strength which increases substantially with natural ageing. It is resistant to 150 °C for long time (10000 minutes) and 260 °C for short time (4 hours). The adhesive performs very well in applications where the two bonded surfaces may expand and contract differentially, since the tape can typically tolerate differential movement (shear or tensile) up to 3 times its thickness. Moreover, it also performs very well in tests, similar to MILSTD 883, which are commonly used to qualify durable products for the electronics industry. Under this testing, protocol bonds are subjected to 1000 hours at 150 °C, 1000 hours at 85 °C and 85% relative humidity, and 1000 hours of thermal shock which cycles hourly from -50°C to 150°C. Figure 4.57 shows the excellent performance of 9460PC in similar testing which involved bonding polyimide to aluminium. Typically the bond strength increases with time due to the more complete wet out of the surfaces.

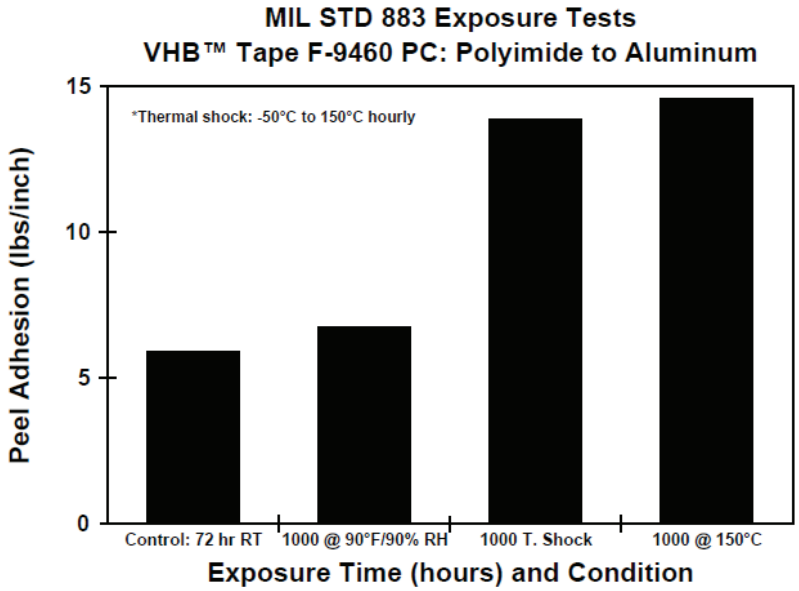


Figure 4.57: Thermal shock properties of 3M VHB 9460 Tape (property of 3M).

Like Y966, this is also a pressure sensitive adhesive transfer tape. It is recommended whenever a high performance adhesive is needed for flexible circuits, aerospace or industrial joining, and high temperature labels. Similarly to Y966, its

ideal application temperature range is 20 to 38°C. Initial tape application to surfaces at temperatures below 10°C is not recommended because the adhesive becomes too firm to adhere readily. However, once properly applied, low temperature holding is generally satisfactory.

As usual, the motherboard has been cleaned with isopropyl alcohol, and, when dry, covered with the double sided adhesive tape at room temperature. Then it has been placed on the flattened Kevlar cloth, rolled, and pressed in place. The final joint has TML = 0.94%, and CVCM = 0.03%, thermal conductivity of 0.16 W/m/K, and CTE = $1.8{\cdot}10^{-4}$ mm/mm/°C.

Table 4.6: Comparison between 3M products: 9460PC and Y966. The Table lists manufacturer's data, except for outgassing values, which have been collected from NASA Outgassing database (9460) and ESA Esmat (966).

| | **VHB 9460PC** | **Y966** | **Note** |
|---|---|---|---|
| **Thickness** | 2 mil | 2 mil | - |
| **Peel Strength to stainless steel** | 12 N/cm | 16 N/cm | Modified ASTM D-3330, 90°peel |
| **Peel Strength to HSE plastic** | 6.6 N/cm | 4.4 N/cm | Modified ASTM D-3330, 90°peel |
| **Temperature Range** | -40°C to +120°C | -40°C to +120°C | Long Term |
| **Outgassing** | TML = 0.85%, CVCM = 0.00% | TML = 0.93%, RML = 0.37%, CVCM = 0.01% | - |
| **Thermal conductivity** | 0.16 W/m/K | 0.18 W/m/K | - |
| **CTE** | 1 ÷ 1.8 m/m/C | 2 ÷ 5.8 m/m/C | - |
| **Dielectric strength** | 1000 V/mil | 1100 V/mil | ASTM D149-92 |

The SDC ambient test verified the adhesion behavior of flexible PI/Cu circuitry when bonded to Kevlar fabric with the aforementioned procedure and bent. No disbonding or defect has been identified, even after operations at 70 °C. The only anomaly was detected during Phase 6, when some air bubbles appeared under the heaters, revealing that some gas was trapped during the gluing process. This was indeed a minor defect of the heater-motherboard bonding, and no dangerous detachment was detected. All heaters continued to perform correctly and there was no disjoining of the smart skin from the support fabric.

The ambient test also confirmed that there is good correspondence between thermocouples and digital sensors, and it evaluated the pros and cons of the control software and graphical user interface. Under the programming (software) perspective, both the firmware and the user interface have satisfied their specifications. Nonetheless, there is room for improvement in two areas: control strategies and HMI. Regarding the control strategies, a first point is, of course, the improvement of

the gradient command control law. To guarantee the functionality of the algorithm, it is probably necessary to add some sort of temperature feedback mechanism in order to correct the duty cycle. Another very relevant aspect to be addressed is the possibility to change (according to the user's needs) the reference temperature sensor used for a certain heater, or to create sensor triplets to be used with a majority voting methodology.

As concerns the human-machine interface, it proved to be a very useful tool in testing, because it offered immediate overview of components' status, and allowed an higher situation awareness with respect to other monitoring methods.

A few additional features could enhance the performance of the GUI. First of all, there is the need for a simple and straightforward data-logging function. At least, this function should save a time-history for all smart skin sensors. Moreover it could save time-referenced data regarding smart skin status (heater status, error messages...) and/or CAN bus traffic. Secondly, some small adjustments in the GUI could be:

- Having a single window for an overall monitoring of the whole system, e.g. a screen with the status (value or error message) for all sensors and heaters. More detailed information on a single element could then be obtained via dedicated sub-menus.
- Adding a function to set up alarms triggered by specific events (threshold crossing, component status change, detection of particular messages on the bus...)
- Showing a clear alert signal when the CAN bus communication is lost (at the present time the interface just freezes in the last valid configuration).
- Allowing the usage of fractional input (at the present time, the HMI accepts only integer inputs).
- Adding a better graphical representation of duty cycle condition (adjust time axis in order to clearly visualize a square wave).
- Improving the send command interface, e.g. using one single heater selection drop down menu (not two), giving each command its own send button, introducing an automatic suppression of all other command input fields when a specific command is being edited.
- Making sure that the GUI aspect is not hardware dependent (in particular, labels must be always readable).
- Paying more attention to the clarity of the interface labels.
- Having the possibility to resize and move windows, and having the possibility to keep multiple windows contemporaneously open (multiple smart skins and/or multiple components).
- Having the possibility to close windows both with a dedicated button and with the usual Windows$^{TM}$X button.

As concerns possible additional functionalities, a number of suggestions arose during the test campaign. It could be useful to add an option to send a command to all devices at the same time (e.g. all heaters - of all smart skins - shut off). Up to now, the interface shows only single-valued (punctual) data: it could be appropriate to show (or give the user tools to build) time history graphs for different variables (e.g. sensors' readings); this could be done, for example, in the aforementioned detailed sub-menus. Finally, more complex control laws, such as those based on PID (proportional-integral-derivative) logics, could be implemented.

The goal of the test campaign was to discover hidden weaknesses that can be solved, therefore increasing the design reliability. COTS electronics was expected to operate accordingly to its specifications without experiencing performance degradations in the thermal-vacuum environment. Smart skins were expected to behave in a nominal way across their whole operative range, i.e. being able to monitor the thermo-mechanical environment and control the temperature distribution onboard the demonstrators. The bonding between the smart skins and their support structures were expected to survive the thermal extremes without sustaining damage.

Generally speaking, the result of the test campaign on the STEPS smart skin was satisfactory and the smart skin design proved to be functional in a relevant environment (vacuum, limit temperatures, coupling with fabrics, bending during operations. . . ).

From an electrical (hardware) point of view, COTS components were used without relevant drawbacks and the design proved to be functional. A possible improvement could be the elimination of cumbersome connectors, perhaps substituting them with Zero Insertion Force clamps, in order to reduce their dimensions and eliminate exposed connections. This solution would also improve the reliability of the mechanical and electrical contact, thus avoiding accidental disconnections. Moreover, the usage of flat connection cables (with thickened terminations suitable for coupling with ZIF connectors) could enhance the ease and reliability of assembly process. The connectors should only fit one way or, as a less appealing an alternative, correct insertion orientation should be clearly indicated on both terminations. Another significant improvement could be the protection of the resistive area for heating devices, e.g. it could be buried in the multilayer stack. Much better, the smart skin could include printed resistors perfectly embedded in the polyimide-copper stack. This aspect of improvement in the design of embedded heating devices is really interesting, especially given the fact that glued heaters can be subject to bad adhesion (due, for examples, to trapped gaseous bubbles), resulting in local overheating and possible damage to the polymeric substrate.

Under a thermomechanical point of view, the bonding of the smart skins to the aluminium panels via Hysol®EA9321, and to the Kevlar fabric via 3M®Y966 showed in both cases the capability to ensure a good adhesion of the flexible motherboard to the different substrates. Both adhesives are well established solutions in the space field: they have well known mechanical and thermal properties, and meet ECSS or NASA requirements regarding outgassing, offgassing, toxicity, and thermal cycling. The experience suggests that acrylic adhesives of the 3M family 100 are well suited for this kind of bonding. The thermal test campaign triggered no

flaw (bubbling, blistering, detachment...) in the bonding layers. Additionally, the bonding process for SDC, with the smart skin on Kevlar cloth was much simpler than the one for the smart skins on aluminium. However, this advantage in terms of process simplification can bring drawbacks in terms of mechanical strength (in particular, peeling resistance, which should be determined before a large scale application of this method). Generally speaking, both bonding procedures are deemed satisfactory at the present time, but they should be subject to further mechanical investigation if a specific mechanical environment is foreseen (as in future smart skin applications).

## 4.3 JPL $\mu$Rover

The work conducted on the microrover did not include environmental tests. Data on the behavior of the Stablcor material is already available ([65], [66]). Since the two prototypes were not in the final MFS configuration, the tests conducted on them were devoted to hardware and software design verification.

However, the activities allowed to verify the big difference in terms of volumes and assembly complexity between the conventional and the MFS approach.

Current methods of integrating avionics in aircrafts and spacecrafts utilize techniques developed in World War II. The standard approach is to partition the electronic functions into several blackboxes that are connected by bulky interface and power cables with two-piece connectors. This approach is robust but carries large weight, volume and touch labor penalties, due to both the hardware construction and the spacing that must be maintained for installation and rework.

The 3D CAD model shows tidy and easy integration of the multifunctional body, where the only bulky components to occupy the chassis are the battery and motors' casings. The two intermediate prototypes, on the other hand, show how crowded and entangled the same system is when manufactured with standard techniques: it is almost impossible to fit all the components in the rover's body.

The work on the $\mu$Rover allowed to explore thoroughly the field of printed circuit boards manufacturing, to practice electrical design techniques, and improve programming skills. Moreover, it was also a reason to study compliant mechanisms, their possible integration in a small system, and their actuation. The result was the design of a working demonstrator rover, capable of remotely operated navigation and manipulation.

The study shows that strong yet light weight structures are achievable for a number of space applications where elements can be fabricated within the limits of commercially available printed circuit board raw material sizes (basically, at the time being, microrovers and nanosatellites or cubesats). The same structure can bear mechanical loads and at the same time have increased heat transfer capabilities for a given mass.

Some aspects still need to be addressed, in particular solder joint reliability for long duration space missions exposed to extreme environments. In fact, the effects of radiation or the ability of structures of this type to shield against low levels of radiation still need to be determined.

# Chapter 5

# Conclusion

The activities described in this thesis responded to all the initial goals. The first goal was to complete the work on the ABB demonstrator, with its integration and testing activity. In fact, the demonstrator was completed and underwent a thermal vacuum test campaign, which led to a positive assessment of the MFS technology. A second goal was to develop the STEPS project, from the design phase to the final prototype verification. Three STEPS demonstrators were designed, manufactured and tested, both in ambient and thermal-vacuum environment. These tests proved the functionality of the design and highlighted area to be further improved. A third goal was to look for additional opportunities to expand the research in the MFS field. This objective was pursued with the acquisition of a funding opportunity under the FP7 (beginning of the ROV-E program) on one side, and with the development of an akin study in collaboration with the Jet Propulsion Laboratory on the other side. The ROV-E activities led to the preliminary design of an improved smart skin concept, and the JPL $\mu$Rover study gave the opportunity to design a tabletop demonstrator and build a first intermediate mock-up. A fourth goal was to introduce a multidisciplinary approach in the design and analysis of multifunctional systems. MDO was studied and then applied for two demonstration loops regarding ABB and STEPS prototypes, and for a re-engineering of the ABB concept. This last study gave interesting results and acted as an input for the ROV-E activities.

The selected technological areas to be investigated in this thesis were: flexible circuitry, embedded thermal hardware, integrated smart devices, diagnostic/control systems, distributed thermal management, and advanced Carbon-Carbon materials with high thermal conductivity. All these topics have been studied and converged into the design of the three more recent MFS demonstrators developed by Thales Alenia Space Italia and JPL.

Regarding the MFS approach in general, the prototypes succeeded in demonstrating the feasibility of two different concepts, that can be customized to create a distributed system with the following characteristics:

- Reduction of I/O count and of conventional cabling systems: the smart skin approach removes a great quantity of wires, substituting them with a single thin ribbon or MB.

- Creation of a modular flexible or rigid-flexible packaging systems, that can fit with different application, architectures and configurations, from telecommunication satellites, to exploration vehicles, to inflatable habitats.
- Spreading of electronics on the supporting structure, freeing up volume that was previously allocated to enclosure boxes, and reducing the mass with respect to an equivalent traditional rigid motherboard.
- Distribution of smart devices, with computation and control capabilities, throughout the system, instead of centralizing them in a single area.
- Inclusion of thermal management solutions, that can go from the passive presence of a tailored high conductivity material to the embedment of heaters piloted by an active control logic handling their behavior.

Two different concepts of integrated multifunctional systems were studied: they are the flat and flexible smart skin layer, and the PCB-based system made of (foldable) structural electronic boards.

Talking about the smart skin, a real breakthrough was the paradigm shift from bulky multifunctional solutions to a very thin and lightweight product that can bring additional functionalities to a variety of structures, with a minimum mass penalty. In particular, the use of flexible polymeric substrates can enable the reel-to-reel fabrication of devices, allowing high volume manufacturing at lower cost. It is also worth mentioning that such materials and production methods open new opportunities to the designer, because they are inherently suitable for atypical applications, like inkjet or screen printed electronics. Under this point of view, the smart skin concept currently under study at Thales Alenia Space Italia is on the cutting edge of MFS research, and has no parallel in the published literature, where flexible polymeric circuitry for space application has been actively proposed only for cable replacement [31]. The smart skin, instead, is a medium to enrich a structure with several features: distributed surface-mounted electronics, distributed sensing networks for health-monitoring function, flat, flexible and modular motherboards providing local interconnects, and integrated heaters to perform thermal control.

At the same time, the foldable structural electronics studied at JPL is also a rather new solution, in the sense that up to now, trials have been made to laminate and include electronics inside structural components, but there is no working example of use of enhanced printed circuit boards as structural components for space applications[1]. In both cases, MFSs tend to minimize part count, mass, and form factor (volume), while at the same time maximizing input/output efficiency, circuit reliability and manufacturability. In particular, under this last point of view, it is interesting to notice that all the prototypes considered in this thesis are immediately manufacturable with existing materials, machines and tools.

The idea of having a modular product is also of great interest, especially when it is possible to depopulate the baseline design in order to reduce the number

[1]Some interesting studies have been conducted on direct printing of electronic circuits on structural elements for the UAV field and in the last months the concept is shifting toward the space sector [86]. In fact, this is also a future evolution of the JPL research branch, that is undertaking the "printed spacecraft" approach.

of sensors and the number of heaters, without any rework or change in the base PCB. This enables an inexpensive spreading of monitoring and control capabilities on very wide surfaces. The modular architecture is also very useful to address the need for rework and repair. In the first idea of MFS, embodied in ABB, the approach assumed to allow correcting anomalies and performing rework or repair was to include bulky fixtures. These fixtures kept in place components that could be dismounted and replaced. However, this idea conflicted with the goal of having a single flat and flexible layer. Therefore the design was changed toward small interchangeable modules that can be easily swapped. In this way, it is possible to test each module and in case of an anomaly discard it prior to integration. Only known good modules are integrated on the spacecraft. In addition, accordingly to good design development practices, spare conductors with open pads can be distributed throughout the module with the difference that, in this case, they would not be used to correct design flaws, but to allow quick modifications in case of faults (e.g. creation of solder jumpers to circumvent damaged areas or intentional cuts). In fact, experience gained during the thermal vacuum test of STEPS prototypes showed that smart skin modules are also quite easy to troubleshoot and rework, even when they have already been bonded to their final substrate. In fact, it was possible to inspect and repair the smart skins onboard SDA and SDB demonstrator without the need to detach them from their support (on the contrary, with a traditional printed circuit board, the procedure would have involved removal and opening of a metal enclosure, and mechanical extraction of the defective component.

It is important to stress the fact that, during the research activity for the development of the STEPS smart skin, the focus was indeed on the single flexible PCB module, to develop its architecture and features, and not on a complete system with a great number of patches. For these reason, in the integration of the final demonstrators, dedicated twisted cables were used to connect the various modules. However, the embodiment of the TAS-I MFS concept has always called for an improvement of integration and assembly activities, even if the reduced I/O count of a smart skin greatly reduces workmanship burden. For this reason, the presence of flat flexible interconnecting cables, terminated with reinforced ends to fit into polarized zero or low insertion force connectors, is a fundamental component of the ROV-E smart skin concept. This solution is the best approach to reduce to the minimum harness handling activities, while at the same time warding off human error.

Going into the details of the ABB application, the concept of a distributed digital temperature sensors network proved to be useful: it can really save mass, volume and costs, since it reduces significantly the health monitoring harness. All wiring bundles are scaled down to a flexible cable. Such a flat ribbon could be used like an inexpensive modular tape running all over the spacecraft. Moreover, there is a great interest in transfering this technology to the testing sector, since a similar solution allows quick test article instrumentation, minimal facility set-up and easy data acquisition. Results from the thermal vacuum test campaign showed that flat flexible electronics was able to withstand vacuum thermal cycling with no damage: the bonding procedure based on Araldite proved effective and showed no degradation even after severe thermal stress. Moreover, usage of COTS electronics

did not hamper the functionality of the breadboard and therefore opens interesting perspectives in three directions:

- It can be a simple and inexpensive solution for testing of space structures, enabling the transition to a direct-to-digital monitoring of the system.
- It can substitute traditional space qualified components in niche application like university nano satellites, research payloads, and expendable instrumentation (e.g. supplementary monitoring like the Exomars heat shield). In certain cases it could represent a cheap redundancy or expansion of an existing monitoring network.
- It can help paving the way toward space qualification of commercially available technologies, in primis few-wires communication protocols and the related hardware that are pervasive in the industry and have shown interesting reliability and flexibility.

The concept of using Carbon-Carbon structures as support panels had interesting potentialities in terms of exploiting the thermal conductivity of the material in order to satisfy thermal dissipation and structural requirements at the same time. To a certain extent, the results of the test campaign are encouraging, since small scale samples exhibited all the foreseen characteristics, but unfortunately the upscaling of the production technology is not yet perfected. In particular, the creation of a monolithic junction between skins and core in a sandwich structure is the weak link, and samples built at an industrially relevant scale have poor mechanical behavior and reduced thermal properties with respect to their smaller counterparts. Given the not completely satisfactory outcome of the study, TAS-I decided to suspend the research in the advanced structures strand, and focus on thermal and electronic aspects.

Regarding STEPS smart skin concept, the flexible MFS modules and their control software were designed and implemented. Three demonstrators were assembled and subject to vacuum and ambient functional tests. The tests confirmed the suitability of flexible electronics substrates for usage in temperature and pressure extremes. It was also possible to verify the good performance of distributed components, that allow a reduced thermal path toward the dissipating radiator surface, and a better thermal control of the system, exploiting the spreading of heating device throughout the control area. In fact, having thermal control hardware disseminated on a wide area, enables targeting thermal control actions to the closest position to the components that requires heating: this can help eliminating the adverse effect of thermal inertia, therefore achieving a better result with a lower dissipation (and in last analysis saving energy), reducing time delays, and having a more accurate temperature control (thus, potentially, a better exploitation of the whole operative temperature envelope of components).

Regarding the application of multidisciplinary analysis and optimization tools, the preparatory work done with demonstrative thermo-structural loops on the ABB and STEPS case studies gave positive results. They gave useful information on the behavior of different algorithms, and on the great advantage coming from a

systematic exploration of the design space: they proved the feasibility of a more thorough, quicker scrutiny of design alternatives that enables the designer to focus on high level choices, while leaving the menial tasks to the machine.

The ABB loop, an a posteriori review of the prototype's design, was based on fine tuning of power dissipated on heaters, and panel's core and skin thicknesses. The evaluation of the thermal performance was done reading temperatures on seventeen points on the upper skin and an equal number on the lower skin, then computing the differences and averaging the values (considering in particular the average values for the two motherboards, for the two DC/DC converters, and an overall figure for the panel). The structural performance was estimated on the basis of maximum x, y, and z displacements. The goals were to keep sensible temperatures inside given ranges, minimize delta temperature across the whole panel (maximize heat rejection capability), and minimize panel's displacements (increase stiffness). The study identified an optimal solution with slightly reduced core height and increased skin thickness. This activity gave a useful overview of issues and good practices related to modeling and simulation for the purpose of performing a multidisciplinary optimization. It was also instrumental in testing different techniques for the design of experiment and optimization phases. Moreover it showed clearly the balancing behavior introduced by an optimization process in presence of several conflicting drivers. Incidentally, the work was also a good demonstration of the necessity of human supervision to make educated choices during the MDO process. Another interesting side effect of the activity was that it helped identifying and correcting modeling errors.

Subsequently, the STEPS demonstration loop was set up as in itinere study to steer the design. It built upon the knowledge gained with the first example. Its goals were the optimization of a small set of parameters in order to satisfy thermal requirements (in terms of minimum gradient and temperature level compliance) and structural ones (in terms of mass budget and survival to launch loads). In this case the objectives were: to ensure the minimum possible temperature difference between the hottest and the coldest point on the motherboard (i.e. a very simple attempt at reducing the temperature gradient across the plane) while keeping the maximum and minimum temperatures in specific ranges, and to minimize the mass of the panel, while enforcing a minimum displacement in the out-of-plane direction. The activity gave reasonable outcomes that were incorporated in the design choices. Under the point of view of exploring potentialities and limitations of multidisciplinary optimization, the work was very useful in highlighting the influence of designer's preferences on the optimization result. It also reinforced the belief that an evaluation of algorithm applicability and performances at the beginning of the study is of paramount importance.

The ABB re-engineering activity had the scope of investigating changes and further developments that could improve the design of ABB and its class of multifunctional structures. In particular, the objective was to enhance the thermal control performance of the outer smart layer of the ABB, in order to both reduce the amount of energy required and obtain a uniform in-plane temperature distribution. Literature shows that there are not many published papers on the multidisciplinary design of MFS. There are few recent works related to the thermal design of such systems ([52], [53], [54], [55]). Those that apply multi-objective optimization to

thermal aspects of multifunctional structures are even more rare are, and they focus in particular on fluidic heat transport ([56], [57]). The reader can also find some papers on the optimization of the mechanical components of multifunctional structures ([58], [59], [60]). These are mainly studies on topology optimization of particular components [58], or studies on core architectures for sandwich structures [59]. Some of them also address the thermal properties of the structural parts [58]. The work on ABB, instead, focused on the application of multiobjective optimization to the selection of a thermal hardware layout and control logic for spaceborne multifunctional structures, in order to minimize energy consumption and, to a lesser extent, to ensure a good temperature distribution. Moreover, the work aimed at giving a quantitative demonstration of the benefits obtainable with PID thermal control logic. Up to now, PID thermal control has only been proposed in a few specific cases with very sensitive payloads ([61], [62], [63]) in order to satisfy very stringent temperature stability requirements, and has never been optimized as a control law for a whole multifunctional assembly to cut the energy budget.

A light, reliable thermal model based on electrical analogy for the multifunctional structure prototype has been created and validated. The model focuses on the description of thermal and electrical phenomena, but leaves aside structural issues. It couples a 3D thermal network with the representations of four different control laws for heater activation, namely ON÷OFF control, proportional logic, proportional-integral-derivative strategy, and the usage of Positive Temperature Coefficient heaters. The parametric model was first validated and correlated through a comparison with simple physical solutions, and then with the actual results of a thermal-vacuum test. This model has then been used to perform multiple runs, with parameters that were determined via design of experiments and multiobjective optimization algorithms.

The three optimization studies (based on genetic algorithms) had the objective of establishing the best heater layout options, identifying the best control strategy in terms both of panel isothermia and energy consumption, and finally fine-tuning the parameters of the selected control strategy, while evaluating the performance of the system in terms of total energy consumption and in-plane temperature uniformity. The study has been able to suggest heater layouts which are more efficient than those obtained with conventional designs: energy consumption can be reduced by a percentage ranging from 26.6% to 39.6%, and temperature uniformity can be improved by 20.3% to 39.6%. The results also highlighted that limitations in heater layout flexibility have a great effect on the ability of the Thermal Control System to maintain a fine regulation of the temperature distribution. After considering the outcomes of the first phase, a finite number of engineeringly viable layouts were chosen, and subsequently used for the rest of the study. These simplified outlines would introduce an acceptable degradation of panel isothermia, but at the same time allow easy manufacturing with a reduction of $17 \div 38$ % of the total heater area. This result clearly shows the advantage that can be obtained with a systematic optimization of the thermal control design. Furthermore, multi-objective optimization techniques have been used, in a quantitative study, to substantiate the convenience of upgrading the thermal control strategy from a simple ON÷OFF logic to a more complex one. In particular, the work has been successful in quantifying the performance improvement that can be obtained with a proportional or proportional-

integral-derivative law. Moreover, the analysis has shown the advantages of an optimized proportional-integral-derivative controller. The energy savings, for the case under study, can reach 34 % compared to a proportional law, and settle around 52 % if compared with the ON÷OFF strategy. These benefits justify the drawback in terms of design complexity, and suggest that, as a general rule, a remarkable improvement of the design can be obtained at the cost of just few hours of computational time (less than 24 hours on a Quad-Core, 3 GHz, 12 MB cache processor). At the end of the process, the multiobjective optimization was able to produce an alternative design that halved the energy consumption and maintained an acceptable temperature distribution with a reduction of 24 % in the required thermal hardware (heater area).

The ROV-E smart skin architecture has been inspired by the results of this multidisciplinary optimization studies. First of all, they made clear the advantages of widespread thermal hardware under precise control, moreover they have shown that the simultaneous adjustment of the geometrical layout, as well as the control strategy and its parameters can lead to substantial energy savings. In particular, it is clear that the granularity of the heating patches foreseen in the ABB re-engineering study can lead to a better control of the in-plane temperature distribution. However, the solutions offered by the algorithms are difficult to put into practice with standard, commercially available thermal hardware. Therefore the ROV-E smart skin is targeted at developing the technology needed for a simple and straightforward implementation of this optimal solution, coupling a widespread thermal control capability with proper control logics.

The ROV-E design phase is not yet complete, but it is possible to remark some of the key aspects of the project. First of all, as with its precursors, the goal of the new smart skin is to reduce volumes occupied by electronic boxes and harness, spreading heating function on a wider area, and introduce a modular design with the possibility to cope with odd and irregular structure shapes. These requirements are accommodated by means of a flexible polymeric substrate that could be polyimide or LCP based. The integration of a dedicated power resistor layer will offer the capability of focusing heating actions only where they are needed, or, on the other hand, of achieving a fine control on the whole system extent. The implementation of few-wires communication protocols enables an increase in the number of monitoring points without a corresponding increase in the number of signal lines. Moreover, having the vast majority of connections already hard-wired inside a module will reduce assembly complexity and human errors during AIT. The small number of connections still needed to guarantee the modularity and interface capabilities of the smart skin will be handled by means of flat ribbon cables and polarized terminations. Another mean of innovation in the ROV-E design is the presence of pervasive computational, sensing and control capabilities nested inside the motherboard substrate thanks to ultra thin chips, therefore able to reduce footprints and thicknesses, and improve the overall flexibility of the final product.

After the work performed with ABB and STEPS test campaigns, the MFS concept can be declared at TRL 5/6 under the thermal point of view. To reach an overall TRL 5/6, further work is needed under the EMI and radiation mitigation

point of view, both in terms of performance tests and design improvements. These aspects are very relevant to ensure the reliability of the smart skin in a satellite- or rover-like environment. In particular, the EMI/EMC are is of primary importance, while radiation mitigation could be not so critical if the envisioned application has a proper fairing able to dampen the radiation dose that reaches the smart skin. Additional mechanical verification activities (e.g. vibration test), could also be interesting. However, this aspect is not so critical, since the smart skin is independent from the supporting structure, and a lot of expertise and test data is already available regarding conventional aluminium or composite structures, which are well known and widely used in the space industry, and reliable electronic components' soldering. Part of this work needed to enhance the smart skin TRL is already taken care of with ROV-E. A particular remark should be made about the possible usage of the smart skin in a deployable or inflatable structure. Its inherent thinness, flexibility and freedom in the geometrical layout make the smart skin an ideal candidate for the addition of health monitoring, thermal and electronic functions in a non-conventional structure. To further develop this potential, a number of issues should be investigated, namely technologies needed to add the smart skin as a further layer in stacks used for inflatable structures (e.g. forming, stitching...), unknown properties of the smart skin (e.g. barrier performance, compatibility with chemicals...), and assembly and repair issues of the layer once it has been embedded.

None of the aspects that still need to be addressed is a show stopper. Most of them have already been dealt with in other sectors, and the main point is to extend the flex circuit culture to the aerospace industry. The initial effort in terms of acquisition of technological know-how and design methodologies[2] can be paid off by the multiple advantages of this solution. Key advantages include large savings, greater than 50%, in cabling mass and volume[3], mass and volume savings in printed circuit boards, exploitation of the third dimension in the layout of circuits, with a product adaptable to small bend radii and odd shapes, greater freedom in the physical location of components, use of distributed active and passive components for sensing or data processing, much lower recurring costs and more repeatable hardware with respect to the conventional approach with electronics boxes and cablings, cost savings through the strong reduction or elimination of workmanship (touch labor).

With respect to terrestrial and civil applications, the smart skin could be a viable option whenever application of health monitoring and thermal control to a structure is required (aeronautic and automotive structures, industrial vessels or tanks...). TRL considerations are very similar to those presented for space applications, with the exception of radiation mitigation issues. As a matter of facts, flexible electronic is already used in civil products, therefore extension of the smart skin usage to terrestrial applications should be favored.

[2]It is undeniable that there are higher non-recurring costs due to the need to acquire: i) competences on the design of flex PCBs, which are completely different from standard or rigid-flex ones, 2) concurrent engineering methodologies with all design disciplines involved at once, and 3) specific design tools for multidisciplinary analysis and optimization.

[3]Manufactured cables have a very high ratio of jacketing material to actual copper conductors, both in weight and volume [31].

On the other hand, as an alternative to the smart skin design, there is the concept of exploiting the mechanical performance of the electronics itself to replace conventional structures. In this field, the JPL study on multifunctional microrovers led to the complete end-to-end design of a working tabletop demonstrator, and the manufacturing, assembly and functional testing of two intermediate mock-ups. After an initial review of small robotic systems and of the technologies needed to put together the final product, the actual design phase took place. The electrical and electronic design of the system included a main controller unit, a wireless communication module, and a DC/DC converter. Additional circuitry was also designed for the actuation of shape memory alloy motors, the handling of a laser module, acquisition of pressure sensors, and battery status monitoring. Under a mechanical point of view, all the flat motherboards composing the rover were modeled in 3D. The mechanical design included the study of a compliant gripper to be used as the end-effector of a five degrees of freedom manipulator arm. Design activities included also the development of all software necessary to handle the $\mu$Rover communication and motion functions. Basically, the code was divided between a low level module resident on the robot, and an high level module resident on the control station (a laptop computer). During the late phases of the design activity, the structural components of a first prototype were built thanks to a stereolithography fabrication process. The prototype was assembled and tested, and used as a workbench for software improvement. In the end, a second mock-up was built, using actual rigid-flex electronics, and proving working integration of all components.

It is worth spending a few words in outlining the situation concerning future work. First of all, activities regarding ROV-E will be carried out until the end of 2013, with the completion of the detailed smart skin design, the manufacturing of a demonstrator, and its test campaign (thermal and mechanical testing). In addition, after the positive outcome of the STEPS program, Thales Alenia Space Italia has decided to apply the technologies studied for the smart skin to a specific design of a distributed thermal control system that will be developed under the new STEPS2 project in the two-year period 2013/2014. Additionally, in the next fiscal year, the JPL $\mu$Rover will be manufactured in its final version. Possible further modifications to the design include the application of inkjet printed electronics directly on the structure.

This thesis dealt with integration of many functions in one single product, and such a proposition can be carried out only by studying the problem from many different points of view, at every stage of the design. Therefore the topic has always been challenging and interesting throughout its development.

Besides the technical results and considerations, the work conducted to create this thesis also included other aspects that have been extremely educational. Those aspects were invaluable lessons on the management of internally and publicly funded research programs. In particular there was the drafting, submission and defense of research proposals at national and European level, which gave a notable experience with all the preparatory activities and the knowledge of the review process needed to submit a winning bid.

Moreover, the work included an inspiring hands-on experience inside the ranks of two world-class level, leading edge players in the aerospace business. The duties covered the whole spectrum of research activities, from planning to testing, from analysis to manufacturing. Of particular interest was also the fine art of dealing with contractors and customers.

In conclusion, this research work has been very enticing and motivating, both for the variety of technical and technological topics encountered, and for the general know-how improvement which is also a priceless professional legacy.

# Further information

## MUSES-CN

The well known Japanese Hayabusa mission, launched on May 9, 2003 from the Japanese Kagoshima launch site, was the first asteroid sample return mission ever attempted. In fact, Hayabusa is mainly famous for the rendezvous with the near-Earth asteroid (25143) Itokawa, a 600 meter sized, potato-shaped celestial body, even if the primary objective of the mission was actually to test new technologies, namely the electric propulsion (ion drive) engines, the autonomous navigation system, the sample collection system, and the re-enter capable sample capsule. Hayabusa also hosted a small exploration robot called MINERVA (MIcro/Nano Experimental Robot Vehicle for Asteroid), a 16-sided prism measuring 12 cm in diameter and 10 centimeters in height, and weighing 591 grams.

What is less known is that, before 2003, the original name of the Hayabusa mission was MUSES-C, but this designation was abandoned after the successful launch of the spacecraft to take on the more flattering Japanese term for "falcon" . Even less known is the fact that, before year 2000, Hayabusa was planned to deploy a small rover supplied by NASA and developed by JPL, called MUSES-CN (N for NASA) [79]. Unfortunately, the rover was canceled by NASA in November 2000 due to budget constraints.

The rover was a direct descendant of the technology used to build the Sojourner rover, while being 10 times less massive. It was conceived to carry three science instruments: a visible imaging camera, a near-infrared point spectrometer, and an alpha X ray spectrometer. Such an imaging system was designed to be capable of making surface texture, composition, and morphology measurements at resolutions better than 1 mm.

The total mass allocated by ISAS for the NASA payload was only 2.7 kg, of which the rover itself occupied only about 1.3 kg, while the remainder of the allowance was consumed by the Orbiter Mounted Rover Equipment (OMRE) located on the main spacecraft to provides the following functions: thermal control of the rover during cruise, mounting of the rover to the spacecraft during launch and cruise, ejection of the rover off the spacecraft towards the asteroid, transmission of commands from the orbiter to the rover and vice versa, and housing of the rover's computer.

Two prototypes of MUSES-CN are shown in Figure 1, while the key rover characteristics are listed in Table 1.

MUSES-CN consisted of a rectangular body, which was $\sim$ 14 x 14 x 6 cm in dimension, and had a very interesting mobility system. Due to the microgravity

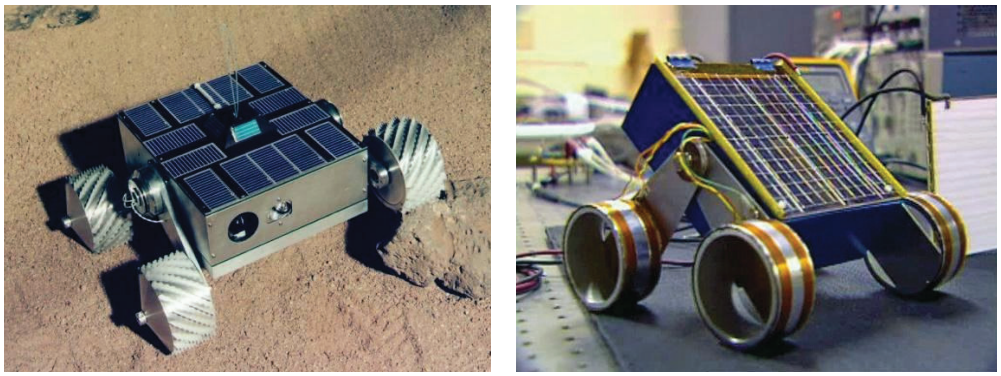

Figure 1: MUSES-CN prototype [79].

Table 1: General characteristics of the MUSES-CN rover.

| **Characteristic** | **Value** |
|---|---|
| Mass | 1300 g |
| Size | 14 x l4 x 6 cm |
| Power capability | 2.3 W |
| Max. velocity (rolling contact in microgravity) | 1.5 mm/s |
| Data rate (at 20 km range) | 4700 bits per second effective rate (9600 baud raw data rate) |

environment on the target asteroid, the maximum speed the rover could travel was about 1.5 mm/s without losing surface contact, and it was designed with the ability to right itself in case it flipped over. Four independent wheels on four posable struts were foreseen to allow the rover both to determine its orientation and to provide the correct attitude for its fixed camera.

The wheels were 6.5 cm in diameter, mounted on struts which extended in pairs from hubs emerging from the geometric center of two opposing 14x6 cm faces of the body. Each strut was 7 cm long from the center of their pivot to the center of the wheel axis. Each strut had 2 motors: one to drive the wheel on its axis and the other to drive the strut around its hub. The shoulder hub included potentiometers for position information. The wheels were complex assemblies of thin conductors and insulators designed to function both as a mechanical wheel and as a proximity sensor to the asteroid surface. The motors selected for the rover were specially developed for this application. They were 3 phase, brushless DC with a specified torque of 1 in-oz (0.07 Kg cm) and a life requirement of l000 hrs within a temperature range of -200 °C to 125 °C. The mass of one motor including its gearbox was only 10 grams.

The mobility subsystem of the rover was designed to support nominal mobility and body-pose functions in full Earth gravity for testing, and also designed to enable significant hops in the expected worst-case microgravity environment of 8 to 80 $\mu$g of surface acceleration coupled with an escape velocity of about 15 - 105 cm/sec. The locomotion subsystem was designed to maintain the mechanical configuration of the rover even if power were lost. Additionally, the rover was designed with the capability to hop in low-gravity, which would have given it the ability to transverse long distances (10 $\div$ 100 m), and maybe enabled it to stay in the Sun longer, to take and transmit more data and avoid thermal cycling. As just mentioned, each wheel assembly also included a sensor to infer contact with the terrain and therefore allow the vehicle to roll on four wheels (instead of just three, which would be the natural state for a four-wheel vehicle without a passive suspension). This sensing system was also useful to detect when one of the wheels had encountered an obstacle, to allow the vehicle to hop with all four wheels pushing so that no significant angular momentum was induced into the body, and to anticipate contact a fraction of a second before landing at the end of a hop.

Thanks to its peculiar mobility system, the rover was a self-righting and upside-down-operable articulated vehicle. For precise motion of the rover to nearby target locations, the rover was planned to use slow rolling. Fine positioning of the rover would have been accomplished by normal rolling motion at slow speeds of 1.5 mm/s or so. At these speeds it was believed that the gravity force (20 $\mu$g nominal) and other forces (e.g. Van der Waals, electrostatic) would allow the rover to maintain at least two wheels in contact with the terrain at all times and therefore enable a quite accurate odometry. For longer-range mobility, hopping or jumps could have been implemented.

The rover was intended to be completely solar powered, with absolutely no battery. Therefore it had an extremely limited power budget, which in turn affected operations, computational power, and communications. Solar panels on four sides of the rover were included to ensure that enough power was always available to the rover, no matter its orientation. The solar cells were selected to be state of

the art multijunction cells with an efficiency of about 25%. A coverglass with an anti-reflective coating was to be put on each cell, and diodes were to be provided for each string to protect against shadows. The solar cell strings were foreseen to produce power between 12 and 30 volts, depending on temperature and load; the maximum power produced by the main panel after radiation exposure and at the high end of the temperature environment was expected to be about 2.5 watts at 1.1 AU. However, no matter what, during periods of eclipse the rover would have been forced to hibernate until sunrise. Upon reawakening, it would then have recovered its state, based on information stored in non-volatile on-board memory as well as on communication with Earth.

Since the rover was designed to transmit its data to the mother spacecraft for relay back to Earth, and since very little non-volatile storage was foreseen on the rover, most data not transmitted to the orbiter at the end of the daily investigation schedule would have been lost. Communication would have been possible thanks to an antenna element mounted on the top face, and therefore, to allow the communication, the rover would have needed to be powered, and oriented in such a way to have a direct line-of-sight with the spacecraft. The MUSES-CN radio was a time-division duplex, L-band (1900 MHz PCS), radio transceiver operating at 9600 symbols per second utilizing non-coherently demodulated, Manchester-coded, binary frequency-shift keying. Its maximum power consumption was 750 mW from a single +5 V DC bus. The rover antenna was a right-hand circularly polarized square patch with an offset-pin feed, fired upon a high-k ceramic substrate.

The peculiar asteroid environment also affected another function of the rover: determination of attitude. Because of the microgravity field, vertical sensing through accelerometers was not viable, since there were no accelerometer which can measure such ranges. Therefore the rover was equipped with optical detectors on all six orthogonal exterior faces, in order to be able to determine the direction to the sun. Additionally the rover had a laser range finder, which enabled it to determine the distance to nearby objects.

The rover's structure was built around an optical bench, made of two panels of aluminum alloy between which the most sensitive equipments were mounted. The electronics board were planned to be mounted on standoffs to the top optical bench panel, while the radio board was to be mounted to the lower optical bench panel. The side panels were connected to the optical bench to act as radiators.

As already mentioned, the rover was planned to carry three science instruments: the visual camera, the near infrared spectrometer, and the alpha X ray spectrometer. A view window on the front face of the rover was foreseen to allow operations for the camera and IR spectrometer, while the AXS sensor would have opened out to the rear of the rover to be placed in contact with rock or regolith by appropriate body/strut motion.

The entire rover system was designed to operate in the temperature range of -180 °C to +110 °C, derived from the worst case situations during the mission. The mechanical environment for the rover was dominated by the vibration environment imposed by the ISAS MV launch vehicle, an all-solid design that called for a l00 Gs load figure. Also, the entire rover was designed to be compatible with a radiation dose of about 25 krad, although many components will tolerate much higher levels.

The rover was equipped with a Synova R3000 32-bit flight processor, and a

radiation hard custom gate-array. In addition, 2Mbytes of rad-hard RAM and l Mbyte of rad-hard EEPROM were provided. The electronics I/O included the camera interface, control of ten 3-phase brushless cryovac motors, IR Spectrometer and alpha X ray spectrometer, and general-purpose digital and analog I/O. The electronics was implemented using double sided chip on board packaging in order to save mass and board area.

A three-position focus camera was used with a flat elliptical gimbaled mirror, which looked out through an optically flat window on the front of the rover to allow looking anywhere up to 30 degrees off-axis. The mirror was included to allow the rover to point the camera to areas that are in focus, instead of focusing on areas that happen to be on a fixed camera pointing axis. The gimbaled mirror could be used to direct light from a wide variety of pointing directions either into the camera or into the IRs pectrometer. This approach also enabled convenient acquisition of panoramic mosaics. The nominal focus range was at about 6 meters. Two closeup lenses could be mechanically inserted into the optical path to change the focus position to 2 meters and 70 mm for extreme closeup images.

The visible camera was a 256 x 256 Active Pixel Sensor (APS) with a custom 30 mm F2 triplet achromat lens. The field-of-view of the camera was 0.1 radians and the resolution was 0.4 mrad/pixel.

# Compliant mechanisms

Traditionally engineered mechanisms are strong, and stiff (rigid), made of many rigid parts connected together with joints. therefore their production is assembly-intensive, and implies undesired aspects such as wear, need for lubrication, backlash...

On the other hand, a Compliant Mechanism (CM) is a one-piece device that has no kinematic joints, and performs its function through the elastic deflection of its members. This kind of mechanisms are strong, and compliant (elastic), they have energy storage capacity, and require no assembly activities. CMs are inspired by nature, which relies on compliance for motion and force transmission for the 90% of all its living creatures (invertebrates).

The advantages of compliant mechanisms are numerous. Having no joints they are characterized by reduced or eliminated assembly, fewer parts, lower cost, and lower weight with respect to analogous classical mechanisms. Moreover, eliminating friction, wear, and backlash, they have increased performance and can effectively transmit the input force or displacement to the output.

There are many potential application for compliant mechanisms, such as MEMS, nano-scale manipulators, and precision tools. What is most relevant is that all their advantages make compliant mechanisms ideally suited for aerospace applications, where low weight and no lubrication are essential. For example, thanks to massive application of distributed compliance, this kind of mechanisms can be used to create shape morphing devices, such as a morphing aircraft wing. It is easy to imagine that a wing foil that changes its shape actively can potentially enhance aircraft performance and improve fuel economy.

Space applications of CMs are also a large and unexplored field. A possible

idea is the application of compliant mechanism technology to the shape morphing of flexible reflectors, e.g. antenna or mirror surfaces. Since the performance of a reflector is strongly linked to its shape, the use of CMs can potentially increase the versatility of radio or optical systems onboard satellites.

Studies have been performed to assess the viability of compliant mechanisms for space usage and several reasons have been outlined in support to the introduction of this new technology [84]. The following is a list of the key aspects:

- Current mechanisms have joints which deteriorate because they are subject to wear and backlash, while CMs do not have such a problem.
- Current mechanisms require lubrication, and this poses some concerns in terms of contamination and outgassing issues. On the other hand CMs require no lubrication and therefore eliminate these concerns.
- Current mechanisms are characterized by large masses, volumes, and costs, while CMs present a reduced part count, simpler geometries and therefore they offer miniaturization and cost saving options. CMs offer an increased number of feasible configurations, and the possibility to integrate multiple functions into one single mechanism.
- Current mechanisms are assumed as rigid, but their stiffness is not infinite, and this can lead to modeling errors. On the contrary, CMs introduce a different approach: distributed compliance is more accurate for analysis than lumped compliance and can be accurately calculated, as a consequence joint and mechanism stiffness can be precisely modeled and predicted.
- Current mechanisms are complex and costly to manufacture and assembly, but CMs can exploit the least expensive manufacturing methods, and require virtually no assembly activities.
- Current mechanisms' dynamics can introduce noise in the feedback loop of control systems, while CMs and their design and analysis tools allow increased predictability and control over mechanisms' mode shapes, natural frequencies, ans stiffnesses.
- Current mechanisms are prone to single point failure modes, but CMs enable redundancy in actuation and motion.
- Current mechanisms can be hampered by inadequate force or torque margin of safety calculation. CMs, on the other hand, can benefit from accurate analysis methods.
- Current mechanisms lack accurate modeling and analysis methods for flexible and large-displacement segments, while CMs intrinsically bring with them proven design and analysis methods.
- Current mechanisms suffer reduced reliability in off-nominal conditions. CMs have analysis methods that provide increased predictability of behavior in off-nominal conditions. Moreover CMs have reduced susceptibility to foreign objects during testing and operation.

- Current mechanisms can be damaged by thermal gradients that cause joint binding or misalignment. CMs, being constructed out of a single continuous material, do not present this problem.

- Current mechanisms present intrinsic defects due to backlash, hysteresis, and joint misalignment, while monolithic nature of CMs eliminates backlash, makes hysteresis predictable, and reduces the need for assembly, thus reducing the possibility of joint misalignment.

Many myths regarding compliant mechanisms can be ruled out [85].

The first one is that flexible structures are prone to fatigue failure with few cycles. In fact, life cycle requirement is a paramount design consideration in the compliant structural optimization. Structures have been developed capable of 220 million morphing cycles while exposed to significant air loads and 600 gs of inertial loads. Sandia National Labs tested a compliant MEMS actuator structure to 10 billion cycles with no failure.

The second myth suggests that flexible structures are not scalable and able to support realistic loads. In fact, compliant mechanisms are scalable, as demonstrated by FlexSys shape morphing technology (dimensions in meters) and micro-scale devices (dimensions in microns).

A third misconception can state that compliant systems are difficult to manufacture. In fact, the design approach and the associated software take into account a desired manufacturing method during structural design and optimization. These mass-manufacturing methods include stamping, casting, extrusion, injection molding, composite molding...

Another myth can argue that compliant mechanism technology is no different than monolithic mechanisms decades old. In fact, the idea of employing elastic strain to generate motions is not new and can be found in household products like shampoo-bottle lids where the lid and the cap are relatively rigid and the flexion is concentrated in a thin flexure hinge (living hinge). Such designs, called "lumped compliance" , result in stress concentrations, limited fatigue life and are not suitable for high load bearing applications. The new approach utilizes distributed compliance, spreading small elastic strain over a large region of the mechanism in a manner that all elements share the load, resulting in large deformations and high fatigue life.

With all that said, compliant mechanisms are an interesting technology useful to expand the design space, and steer space mechanisms toward ever more adaptive and autonomous devices.

# Acronyms & Abbreviations

| | |
|---|---|
| ABB | *Advanced BreadBoard* |
| ABS | *Acrylonitrile Butadiene Styrene* |
| ACK | *ACKnowledge* |
| ACS | *Attitude Control System* |
| ADC | *Analog to Digital Converter* |
| ADP | *Atmospheric Downstream Plasma* |
| AFRL | *Air Force Research Laboratory* |
| AFRL/PL | *Air Force Research Laboratory/Philips Laboratory* |
| AIAA | *American Institute of Aeronautics and Astronautics* |
| AIT | *Assembly Integration and Testing* |
| AMGA | *Archive-based Micro Genetic Algorithm* |
| AS&T | *Advanced Systems and Technology* |
| ASA | *Adaptive Simulated Annealing* |
| ASIG | *Autocatalytic Silver and Immersion Gold* |
| ASTM | *American Society for Testing and Materials* |
| ATDS | *Advanced Technology Demonstration Spacecraft* |
| ATeX | *Advanced Tether eXperiment* |
| AU | *Astronomical Unit* |
| AWSM | *Adaptive Weighted Sum Method* |
| AXS | *Alpha X-ray Spectrometer* |
| | |
| BB | *BreadBoard* |
| BB1 | *BreadBoard 1* |
| BB2 | *BreadBoard 2* |
| BB3 | *BreadBoard 3* |
| BB4 | *BreadBoard 4* |
| BCB | *BenzoCycloButene* |
| BLF | *Buckling Load Factors* |
| BMDO | *Ballistic Missile Defense Office* |
| BO-PET | *Biaxially-Oriented PolyEthylene Terephthalate* |
| BOL | *Begin Of Life* |
| BoM (or BOM) | *Bill of Materials* |

| | |
|---|---|
| C/C | *Carbon-Carbon* |
| C&DH | *Command and Data Handling* |
| CAD | *Computer Aided Design* |
| Caltech | *California Institute of Technology* |
| CAN | *Controller Area Network* |
| CBGA | *Ceramic Ball Grid Array* |
| CCD | *Central Composite Design* |
| CCL | *Carbon Core Laminate* |
| CCR | *Carbon-Carbon Radiator* |
| CDMU | *Command and Data Management Unit* |
| CE | *Concurrent Engineering* |
| CE | *Conducted Emission* |
| CFRP | *Carbon Fibre Reinforced Plastic* |
| CIC | *Copper-Invar-Copper* |
| CIS | *Copper Indium Selenide* |
| CM | *Common Mode* |
| CM | *Compliant Mechanism* |
| CMOS | *Complementary Metal Oxide Semiconductor* |
| CMP | *Chemical Mechanical Polishing* |
| CMST | *Centre for Micro Systems Technology* |
| CO | *Collaborative Optimization* |
| COTS | *Commercial Off The Shelf* |
| CRS | *Coarse Rate Sensors* |
| CS | *Conducted Susceptibility* |
| CSSO | *Concurrent Subspace Optimization* |
| CTE | *Coefficient of Thermal Expansion* |
| Cu | *Copper* |
| CVCM | *Collected Volatile Condensible Material* |
| | |
| DAQ | *Data AcQuisition* |
| DARPA | *Defense Advanced Research Project Agency* |
| DBB | *Demonstrator BreadBoard* |
| DC | *Direct Current* |
| DCE | *Dry Chemical Etching* |
| DH | *Denavit-Hartenberg* |
| DM | *Differential Mode* |
| DoD | *Department of Defence* |
| DoE | *Design of Experiments* |
| DOF (or DoF) | *Degree Of Freedom* |
| DRAM | *Dynamic Random Access Memory* |
| DS1 | *Deep Space 1* |
| DS2 | *Deep Space 2* |
| DSE | *Design Space Exploration* |
| | |
| E3 (or EEE) | *Electromagnetic Environmental Effects* |
| EC | *European Commission* |

| | |
|---|---|
| ECD | *Electro Chromic Devices* |
| ECSS | *European Cooperation for Space Standardization* |
| EDL | *Entry Descent and Landing* |
| EMC | *Electro Magnetic Compatibility* |
| EMI | *Electro Magnetic Interference* |
| EMP | *Electro Magnetic Pulse* |
| ENPIG | *Electroless Nichel/Palladium and Immersion Gold* |
| EO-1 | *Earth Observing-1* |
| EPS | *Electrical Power Subsystem* |
| ES | *Evolutionary Strategy* |
| ESA | *European Space Agency* |
| ESD | *Electro Static Discharge* |
| ESR | *Equivalent Series Resistance* |
| ESTEC | *European Space Agency Technology Center* |
| FAST | *Fast Auroral Snapshot Explorer* |
| FEM | *Finite Element Model* |
| FFC | *Flat Flexible Cable* |
| FP | *Framework Programme* |
| FPCB | *Flexible Printed Circuit Board* |
| GA | *Genetic Algorithm* |
| GLAST | *Gamma-ray Large Area Space Telescope (Fermi Gamma-ray Space Telescope)* |
| GMM | *Geometrical Mathematical Model* |
| GSTP | *General Support and Technology Programme* |
| GUI | *Graphical User Interface* |
| GUIDE | *GUI Development Environment* |
| GYR | *GYRoscope* |
| H/C | *HoneyComb* |
| HDI | *High Density Interconnects* |
| HE | *High Energy* |
| HMC | *Horizontal Mounted Cube* |
| HMI | *Human Machine Interface* |
| HP | *Heat Pipe* |
| HSE | *High Surface Energy* |
| HVLP | *High Volume Low Pressure* |
| I/F | *InterFace* |
| I2C (or $I^2C$ or IIC) | *Inter-Integrated Circuit* |
| IAD | *Inflatable Aerodynamic Decelerator* |
| IAS | *Integrated Avionics System* |
| IC | *Integrated Circuit* |

| | |
|---|---|
| IO (or I/O) | *Input Output* |
| ISAS | *Institute of Space and Astronautical Science* |
| ISR | *Interrupt Service Routine* |
| ISS | *International Space Station* |
| ITT | *Invitation To Tender* |
| JPL | *Jet Propulsion Laboratory* |
| KKT | *Karush Kuhn Tucker* |
| LAN | *Local Area Network* |
| LaRC | *Langley Research Center* |
| LBF | *Long Beam Flexure* |
| LCD | *Liquid Crystal Display* |
| LCP | *Liquid Crystal Polymer* |
| LDO | *Low Drop Out* |
| LFSA | *Lightweight Flexible Solar Array* |
| LIF | *Low Insertion Force* |
| LIN | *Local Interconnect Network* |
| LMA | *Lockheed Martin Astronautics* |
| LN2 | *Liquid Nitrogen* |
| LOS | *Line Of Sight* |
| LP | *Linear Programming* |
| M3D | *Maskless Mesoscale Material Deposition* |
| MB | *MotherBoard* |
| MCM | *Multi Chip Module* |
| MCO | *Mars Climate Orbiter* |
| MCU | *Main Controller Unit* |
| MDA | *Missile Defense Agency* |
| MDO | *Multidisciplinary Design Optimization* |
| MEMS | *Micro Electro Mechanical Systems* |
| MFCBS | *Multifunctional Composite Bus Structure* |
| MFS | *Multi Functional System (or Structure)* |
| MGS | *Mars Global Surveyor* |
| MINERVA | *MIcro/Nano Experimental Robot Vehicle for Asteroid* |
| MIT | *Massachusetts Institute of Technology* |
| MLI | *Multi Layer Insulation* |
| MMC | *Metal Matrix Composites* |
| MMOD | *MicroMeteoroid and Orbital Debris* |
| MPL | *Mars Polar Lander* |
| MRO | *Maintenance Repair and Overhaul* |
| MSDO | *Multidisciplinary System Design Optimization* |
| MSL | *Mars Science Laboratory* |
| MSR | *Mars Sample Return* |

| | |
|---|---|
| MUSES-C | *Mu Space Engineering Spacecraft C* |
| NACK | *Negative ACKnowledge* |
| NASA | *National Aeronautics and Space Administration* |
| NBI | *Normal Boundary Intersection* |
| NCGA | *Neighborhood Cultivation Genetic Algorithm* |
| NEAR | *Near Earth Asteroid Rendezvous* |
| Nitinol | *Nichel Titanium Naval Ordinance Laboratory* |
| NLPQL | *Non-Linear Programming by Quadratic Lagrangian* |
| NMOS | *N-type Metal Oxide Semiconductor* |
| NMP | *New Millennium Program* |
| NRO | *National Reconnaissance Office* |
| NTC | *Negative Temperature Coefficient* |
| OFET | *Organic Field Effect Transistor* |
| OLED | *Organic Light Emitting Diode* |
| OMRE | *Orbiter Mounted Rover Equipment* |
| OPI | *Openings Per Inch* |
| OPVC | *Organic PhotoVoltaics Cell* |
| P/L | *PayLoad* |
| PARC | *Palo Alto Research Laboratory* |
| PCB | *Printed Circuit Board* |
| PCS | *Personal Communication Service* |
| PCU | *Power Control Units* |
| PGA | *Pin Grid Array* |
| PI | *PolyImide* |
| PID | *Proportional Integral Derivative* |
| PLM | *PayLoad Module* |
| PSD | *Power Spectral Density* |
| PTC | *Positive Temperature Coefficient* |
| PTF | *Polymer Thick Film* |
| PTFE | *PolyTetraFluoroEthylene* |
| PTH | *Plated Through Hole* |
| PWM | *Pulse Width Modulation* |
| QI | *Quasi Isotropic* |
| R&D | *Research and Development* |
| RADHAZ | *RADiation HAZard* |
| RAMS | *Reliability Availability Maintainability and Safety* |
| RE | *Radiated Emission* |
| RF | *Radio Frequency* |

| | |
|---|---|
| RFI | *Radio Frequency Interference* |
| RH | *Relative Humidity* |
| RM | *Rover Module* |
| RML | *Recovered Mass Loss* |
| RMS (or rms) | *Root Mean Square* |
| RS | *Radiated Susceptibility* |
| RTOS | *Real Time Operating System* |
| RTR | *Reel-To-Reel (or Roll-to-Roll)* |
| RTU | *Remote Terminal Unit* |
| RWL | *Reaction Wheel* |
| | |
| S/C (or SC) | *SpaceCraft* |
| SA | *Simulated Annealing* |
| SA | *Solar Array* |
| SAMPLEX | *Solar Anomalous and Magnetospheric ParticLe EXplorer* |
| SAS | *Sun Acquisition Sensor* |
| SBA | *Small Business Administration* |
| SBF | *Short Beam Flexure* |
| SBIR | *Small Business Innovation Research* |
| SCL | *Serial CLock* |
| SDA | *STEPS Demonstrator A* |
| SDA | *Serial DAta* |
| SDB | *STEPS Demonstrator B* |
| SDC | *STEPS Demonstrator C* |
| SERMS | *Studio degli Effetti delle Radiazioni sui Materiali per lo Spazio* |
| SJR | *Solder Joint Reliability* |
| SLP | *Sequential Linear Programming* |
| SMA | *Shape Memory Alloy* |
| SMD | *Surface Mount Device* |
| SPI | *Serial Peripheral Interface* |
| SQP | *Sequential Quadratic Programming* |
| SRAM | *Static Random Access Memory* |
| SSD | *Solid State Drive* |
| SST | *Soluble Support Technology* |
| ST5 | *Space Technology 5* |
| STEPS | *Sistemi e Tecnologie per l'EsPlorazione Spaziale* |
| STEX | *Space Technology EXperiment* |
| STR | *Star TRacker* |
| STRP | *Specific Targeted Research Projects* |
| STRV-1d | *Space Technology Research Vehicle-1d* |
| STTR | *Small business Technology TRansfer* |
| SVM | *SerVice Module* |
| SWAS | *Submillimeter Wave Astronomy Satellite* |

| | |
|---|---|
| TAS | *Thales Alenia Space* |
| TAS-I | *Thales Alenia Space Italia* |
| TB | *Thermal Balance* |
| TBC | *To Be Confirmed* |
| TC | *TeleCommand* |
| TC | *ThermoCouple* |
| TCR | *Temperature Coefficient of Resistance* |
| TCS | *Thermal Control Subsystem* |
| TFP | *Thick Film Polymer* |
| TFT | *Thin Film Transistor* |
| THD | *Through Hole Device* |
| TM | *TeleMetry* |
| TML | *Total Mass Loss* |
| TMM | *Thermal Mathematical Model* |
| TRACE | *Transition Region And Coronal Explorer* |
| TRL | *Technology Readiness Level* |
| TS-ETA | *Thermal Systems Engineering Technological Area* |
| TSP | *Twisted Shielded Pair* |
| TT&C | *Telemetry Tracking and (tele)Command* |
| TV | *Thermal Vacuum* |
| TVC | *Thermal Vacuum Chamber* |
| TVT | *Thermal Vacuum Test* |
| TWT | *Travelling Wave Tube* |
| UAV | *Unmanned Aerial Vehicle* |
| USB | *Universal Serial Bus* |
| USDC | *United States Display Consortium* |
| UTCP | *Ultra Thin Chip Package* |
| UV | *UltraViolet* |
| VCM | *Volatile Condensable Material* |
| VP | *Volts (Peak)* |
| VPP | *Volts (Peak-to-Peak)* |
| WA | *Water Absorption* |
| WAN | *Wide Area Network* |
| WIRE | *Wide field InfraRed Explorer* |
| WVR | *Water Vapour Regained* |
| ZIF | *Zero Insertion Force* |

# Bibliography


[1] B. Muirhead *Technology Thrust Areas for Mass Constrained Spacecraft*. Proceedings of AIAA/DARPA Meeting on Lightweight Satellite Systems, 4 - 6 August 1987, Monterey, California.

[2] D. Leonard, and D. Kiron *Managing Knowledge and Learning at NASA and the Jet Propulsion Laboratory (JPL)*. Harvard Business School, 9-603-062, Rev. October 29, 2002.

[3] D. J. Inman, E. J. Ruggiero, J. H. Lalli, and L. Lee *Concept Paper A07: Composite Materials with Embedded Sensing*. CANEUS Organization, 2004.

[4] J. Foster, and G. Aglietti *Strategies for Thermal Control of a Multifunctional Power Structure Solar Array*. Journal of Aerospace Engineering, 25(3), 454-462, 2012.

[5] E. Fosness, J. Guerrero, K. Qassim, and S.J. Denoyer *Recent Advances In Multi-Functional Structures*. Air Force Research Laboratory, 2000.

[6] E. Ponslet, F. Biehl, and E. Romero *Carbon-Carbon Composite Closeout Frames for Space Qualified, Stable, High Thermal Conductivity Detector Support Structures*. HYTEC Inc., 2000.

[7] E. Zeminiani *Technological Survey of Multifunctional Structures - Integration and Testing of a Demonstrator Panel*. Tesi di Laurea Specialistica in Ingegneria Aerospaziale, Politecnico di Torino, 2009.

[8] R.J. Niccum, J.B. Munson, and L.L. Rueter *Investigation of Kevlar Fabric-Based Materials fo Use with Inflatable Structures*. Sheldahl, Inc. and Langley Research Center, NASA, 1977.

[9] A.L. Hutchings, and R.D. Braun *Experimental Determination of Material Properties for Inflatable Aeroshell Structures*. MS Special Problems Report, Space Systems Design Lab - Guggenheim School of Aerospace Engineering - Georgia Institute of Technology, 2009.

[10] M.C. Lindell, S.J. Hughes, M. Dixon, and C.E. Willey *Structural Analysis and Testing of the Inflatable Re-entry Vehicle Experiment (IRVE)*. AIAA Paper, 2006.

[11] S.M. Murman, and S.A. Suresh *Modeling Effective Stiffness Properties of IAD Fabrics*. AIAA Paper 2011-2568, 2011.

[12] E.I. Madaras, R.F. Anastasi, J.P. Seebo, G. Studor, D.L. McMakin, R. Nellums, and W.P. Winfree *The Potential for Imaging In Situ Damage in Inflatable Space Structures*. Proceedings of the 34th Annual Review of Progress in Quantitative Nondestructive Evaluation, Volume 975, pp. 437-444, 2008.

[13] K.J. Kennedy *Inflatable Habitats Technology Development*. NASA Johnson Space Center Technical Memorandum, 2000.

[14] S.L. Veldman, and C.A. Vermeeren *Inflatable Structures in Aerospace Engineering - An Overview*. Proceedings of the European Conference on Spacecraft Structures, Materials and Mechanical Testing, 29 November - 1 December 2000, ESTEC.

[15] M.C. Lou *Development and Application of Space Inflatable Structures*. 22nd International Symposium on Space Technology and Science, 28 May - 4 June 2000, Morioka, Japan.

[16] S. Mileti, G. Bitetti, and M. Marchetti *Reliable numerical approach for a design of an inflatable Moon/Mars habitat based on material tests in the SAS simulator*. Proceedings of the European Conference on Spacecraft Structures, Materials and Mechanical Testing 10 - 12 May 2005, Noordwijk, The Netherlands.

[17] R. Destefanis, E. Amerio, M. Briccarello, M. Belluco, M. Faraud, E. Tracino, and C. Lobascio Space Environment Characterisation of Kevlar®: Good For Bullets, Debris and Radiation Too. Proceedings of the 11th International Symposium on Materials in a Space Environment, 15 - 18 September 2009, Aix-en-Provence, France.

[18] D.M. Barnett, and S.P. Rawal *Multifunctional Structures Technology Demonstration on New Millennium Program (NMP) Deep Space 1 (DS1): DS1 Technology Validation Report*. Lockheed Martin Astronautics Division & JPL, 1999.

[19] European Space Agency *Multifunctional Structure For Hydrogen Storage: Executive Summary*. ESTEC, 2005.

[20] G. Birur *Thermal Control of Small Spacecraft Using Single and Two-Phase Fluid Loops*. International Two-Phase Thermal Control Technology Workshop European Space Agency Technology Center, Noordwijk, The Netherlands - September 15-17, 2003.

[21] N.M. Teti *LA-II Thermal Coating Validation Report*. Swales Aerospace, 2002.

[22] A. Little, R. Estes, D. Neil, D. Rosenbaum, and N. Abedin *Geostationary Tropospheric Pollution Satellite (Geo Tropsat) - System Study Report*. NASA Langley Research Center, 1998.

[23] S.C. Hayden, A.J. Sweet, S.E. Christa, D. Tran, and S. Shulman *Advanced Diagnostic System on Earth Observing One*. American Institute of Aeronautics and Astronautics, 2005.

[24] C.P. Minning, and P. Luers *The New Millennium Program: Validating Advanced Technologies for Future Space Missions*. NASA, 1998.

[25] F.K. Li *New Millennium Program Overview*. Jet Propulsion Laboratory, 2000.

[26] D. Crisp, and C. Raymond *The NASA New Millennium Program: Advanced Technologies For Future Science Missions*. Jet Propulsion Laboratory, 2000.

[27] D. Butler *Carbon-Carbon Radiator*. NASA Goddard Space Flight Center - EO1 Mission Technology Forum, 2001.

[28] N. Teti *AZW/LA-II Low Alpha Inorganic White Thermal Coating*. NASA Goddard Space Flight Center - EO1 Mission Technology Forum, 2001.

[29] J. Lyons, and B. Carpenter *Lightweight Flexible Solar Array (LFSA)*. NASA Goddard Space Flight Center - EO1 Mission Technology Forum, 2001.

[30] M. Martin, P. Klupar, S. Kilberg, and J. Winter *Techsat 21 and Revolutionizing Space Missions Using Microsatellites*. American Institute of Aeronautics and Astronautics, 2001.

[31] D.M. Barnett, H.K. Uka, J. Guerrero, B. Arritt, K. Qassim, A. Singh, and A. Malshe *Flexible Circuit Applications in Flight Hardware*. 5th AIAA Aviation, Technology, Integration, and Operations (ATIO) Conference, 26 - 29 September 2005, Arlington, Virginia.

[32] M. Pimprikar *NT Space Applications For Defense*. Centre for Large Space Structures and Systems (CLS3), 2005.

[33] D. Brennan, R. Lyons Jr., M. Porter, R. Shendock, S.J. Bitar, F.Sanidad, and F.J. Looft *Space Technology 5 (ST5) Spacecraft Modeling*. Worcester Polytechnic Institute, 2004.

[34] C. Menon, T. Seidl, and M. Broschart *Biomimetic Approach To Advanced Space Missions*. 5th IAA Symposium On Realistic Near-Term Advanced Scientific Space Missions, 2007.

[35] M. Gottero *Development Of Multifunctional Systems At Thales Alenia Space*. Thales Alenia Space, 2007.

[36] Gottero, Fornari, and Zordan *BB1/BB2 Conceptual Design*. Alcatel Alenia Space, 2006.

[37] Girotto, Gottero, and Fornari *BB1 & BB2 final design and manufacturing*. Alcatel Alenia Space, 2006.

[38] S. Brunner *Manufacturing Plan BB1/BB2 Mechanical Design*. HTS GmbH, 2006.

[39] M. Gottero, and S. Tavera *Advanced Thermomecanical Systems For High Dissipations And Health Management: MFS DBB Test Specifications And Plan*. Alcatel Alenia Space, 2007.

[40] L. Andrioli, and M. Gottero *Advanced thermo-mechanical systems for high-dissipations and health management: trade-off analyses*. Alcatel Alenia Space, 2006.

[41] M. Gottero *Multifunctional Systems (Final 2007 PCC: research in Satellite, Platform & Infrastructures)*. Thales Alenia Space, 2007.

[42] M. Gottero, J. Ralph, G. Atxaga, U. Dehne, S. Fernández, and L. González *MULFUN: Technology Transfer Report* MULFUN-D6.11, 2008.

[43] G. Atxaga et al. *MULFUN: Multifunctional Structures - 2nd Year Progress Report*. NASMET - Tecnalia (MULFUN-PR-24M), 2006.

[44] R. John *MULFUN: Multifunctional structures - Test report: WP2/3, Panel with passive thermal control*. HTS GmbH, 2007.

[45] J. Sobieszczanski-Sobieski, J. Barthelemy, and G. Giles *Aerospace Engineering Design by Systematic Decomposition and Multilevel Optimization*. Proceedings of the 14th International Council of the Aeronautical Sciences (ICAS), September 1984, Toulouse, France.

[46] AIAA Technical Committee on Multidisciplinary Design Optimization *Current State of The Art on Multidisciplinary Design Optimization (MDO)*. White Paper, September 1991.

[47] H. Hopkins *Investigation of Direct and Indirect Optimization Algorithms for Aerospace Structures*. Air Force Institute of Technology, Master Thesis, 1990.

[48] D. N. Kumar *Optimization Methods: Advanced Topics in Optimization - Direct and Indirect Search Methods*. Indian Institute of Science Bangalore, Lecture Notes, 2007.

[49] R.M. Lewis, V. Torczon, and M.W. Trosset *Direct Search Methods: Then and Now*. NASA ICASE Report, May 2000.

[50] A. Mannarelli *Modellizzazione e Ottimizzazione Multidisciplinare di Strutture Multifunzionali per Applicazioni Spaziali*. Politecnico di Torino, Master Thesis, 2010.

[51] A. Iurlaro *Strutture Multifunzionali per Applicazioni Spaziali: Creazione del Modello e Ottimizzazione*. Politecnico di Torino, Master Thesis, 2011.

[52] S. Zhang, X. Cao, Y. Luan, X. Ma, X. Lin, and X. Kong *Preparation and Properties of Smart Thermal Control and Radiation Protection Materials for Multi-functional Structure of Small Spacecraft*. Journal of Materials Science and Technology, Vol. 27, Issue 10, October 2011, pp. 879, 884.

[53] J.A. Foster, and G.S. Aglietti *The Thermal Environment Encountered in Space by a Multifunctional Solar Array*. Aerospace Science and Technology, Vol. 14, January 2010, pp. 213, 219.

[54] D.T. Queheillalt, G. Carbajal, G.P. Peterson, and H.N.G. Wadley *A Multifunctional Heat Pipe Sandwich Panel Structure*. International Journal of Heat and Mass Transfer, Vol. 51, June 2007, pp. 312, 326.

[55] S.P. Rawal, D.M. Barnett, and D.E. Martin *Thermal Management for Multifunctional Structures*. IEEE Transactions on Advanced Packaging, Vol. 22, No. 3, August 1999, pp. 379, 383.

[56] A.D. Williams, R.L. Underwood, and B.J. Arritt *Biologically Inspired Multifunctional Composite Panel with Integrated Thermal Control*. 51st AIAA/ASME/ASCE/AHS/ASC Structures, Structural Dynamics, and Materials Conference, April 2010, Orlando, Florida.

[57] C.S. Roper *Multiobjective Optimization for Design of Multifunctional Sandwich Panel Heat Pipes with Micro-Architected Truss Cores*. International Journal of Heat and Fluid Flow, Vol. 32, July 2010, pp. 239, 248.

[58] V.J. Challis, A.P. Roberts, and A.H. Wilkins *Design of Three Dimensional Isotropic Microstructures for Maximized Stiffness and Conductivity*. International Journal of Solids and Structures, Vol. 45, 2008, pp. 4130, 4146.

[59] X.H. Tan, and A.K. Soh *Multi-Objective Optimization of the Sandwich Panels with Prismatic Cores Using Genetic Algorithms*. International Journal of Solids and Structures, Vol. 44, 2007, pp. 5466, 5480.

[60] L. Valdevit, A.J. Jacobsen, J.R. Greer, and W.B. Carter *Protocols for the Optimal Design of Multi-Functional Cellular Structures: From Hypersonics to Micro-Architected Materials*. Journal of The American Ceramic Society, Vol. 94, Issue Supplement s1, June 2011, pp. s15, s34.

[61] C. Pan, Q. Youshan, L. Huijuan, and T. Jiahai *Design and Implementation of Cooling System for Focal Plane Assembly of Observation Camera in Astronomical Satellite*. 1st IEEE International Conference on Electronics, Communications and Control (ICECC), September 2011, Ningbo, China.

[62] C. Leroy, M. Maisonneuve, M. Piat, J.F. Trouilhet, D. Pearson, C. Camier, and S. Guibert *Simulation of the Planck-HFI Thermal Control System*. Proceedings of SPIE (International Society for Optics and Photonics), Vol. 7017, 2008, pp. 701713-1, 701713-8.

[63] D. Valentini, M. Vacance, D. Battaglia, B. Pieper, and J.M. Niot *GOCE Instrument Thermal Control*. 36th International Conference on Environmental Systems, July 2006, SAE Technical Paper 2006-01-2044.

[64] D. Hunter *Integrated Avionics System (IAS), Integrating 3-D Technology on a Spacecraft Panel*. Proceedings of IPACK'03 ASME International Electronic Packaging Conference, 6 - 11 July, Maui, Hawaii.

[65] D. Schatzel *Multi-Functional Spacecraft Structures Integrating Electrical and Mechanical Functions*. Proceedings of the 2007 IEEE Aerospace Conference, 3 - 10 March 2007, Big Sky, Montana.

[66] D. Schatzel *Reliability of Carbon Core Laminate Construction in Printed Circuit Boards Utilizing Stablcor$^{TM}$*. Jet Propulsion Laboratory/California Institute of Technology, JPL Publication 09-37 12/09, 2009.

[67] R. John, G. Atxaga, H. J. Frerker, and A. Newerla *Advancement of Multifunctional support structure technologies (AMFSST)*. EDA Publishing/THERMINIC, 2007.

[68] M. Gottero *High Dissipations Management: Survey Of Multifunctional Structures Development*. Alcatel Alenia Space Technical Memorandum, 2006.

[69] Prakash et al *Light-weight structural materials with integral radiation shielding, thermal control and electronics*. NASA Langley Research Center Technical Memorandum, Hampton, 1999.

[70] F. Barlow, A. Lostetter, A. and Elshabini *Low cost flex substrates for miniaturized electronic assemblies*. Microelectronics Reliability 42 (2002) 1091-1099, Elsevier 2002.

[71] M. Yan et al *Lexan for Organic Electronics*. proceedings of the 5th USDC Annual Flexible Displays and Microelectronics Conference, 7 - 9 February 2006, Phoenix, Arizona.

[72] E. Cleland, R.F. Muraca, A.A. Koch, and J.S. Whittick *Polymers for Spacecraft Hardware*. NASA JPL Technical Progress Report No. 32 February 15, 1967.

[73] V. Cascioli *Design and Realization of a Space Multifunctional Structure*. Universitá Degli Studi Di Perugia - PhD Thesis, 2009.

[74] T. Dingemans et al *Liquid-Crystal Thermosets, a New Generation of High-Performance Liquid-Crystal Polymers*. NASA Langley Research Center - NASA Tech Briefs, February 2004.

[75] M. Nakayama, T. Yamamoto, R. Turunen, and D. Numakura *Flexible Led Arrays Made by All Screen Printing Process*. IPC Printed Circuit Expo/APEX and the Designers Summit, 29 March - 2 April 2009, Las Vegas, Nevada.

[76] D. Numakura *Advanced Screen Printing - Practical Approaches for Printable & Flexible Electronics*. Proceedings of the 3rd International Microsystems, Packaging, Assembly & Circuits Technology (IMPACT) Conference, 22 - 24 October 2008, Haverhill, MA.

[77] K.H. Choi, M.N. Awais, H.C. Kim, and Y.H. Doh *Cost-effective printed memristor fabrication and analysis*. 13th International Workshop on Cellular Nanoscale Networks and Their Applications (CNNA), 29 - 31 August 2012, Turin, Italy.

[78] J. Vanfleteren *Chip embedding and fabrication of package stacks using Ultra-Thin Chip Packages (UTCPs)*. Proceedings of International Microelectronics And Packaging Society (IMAPS) Conference, 9 June 2011, Eindhoven, Benelux.

[79] B.H. Wilcox, and R.M. Jones *The MUSES-CN nanorover mission and related technology*, Proceedings of the IEEE Aerospace Conference, 18 - 25 March 2000, Big Sky, Montana.

[80] R.N. Jazar *Theory of Applied Robotics - Kinematics, Dynamics, and Control*, Second Edition, ISBN 978-1-4419-1749-2 Springer 2010.

[81] P.I. Corke *Robotics, Vision and Control*, Springer 2011, ISBN 978-3-642-20143-1.

[82] K.J. Lu, and S. Kota *Topology and Dimensional Synthesis of Compliant Mechanisms Using Discrete Optimization*, ASME Journal of Mechanical Design, Vol. 128 Issue 5, pp. 1080 - 1091, September 2006.

[83] S. Zirbel *Compliant Space Mechanisms*, NASA Space Grant Project Report, Jet Propulsion Laboratory/California Institute of Technology, August 2012.

[84] R.M. Fowler, L.L. Howell, and S.P. Magleby *Compliant space mechanisms: a new frontier for compliant mechanisms*, Mechanical Sciences, 2, 205-215, 2011.

[85] B. Trease *Compliant Space Mechanisms*, Internal Presentation, Compliant Systems Design Laboratory (University of Michigan), Jet Propulsion Laboratory (California Institute of Technology), October 12, 2011, Pasadena, California.

[86] A.J. Lopes, E. MacDonald, and R.B. Wicker, *Integrating stereolithography and direct print technologies for 3D structural electronics fabrication*. Rapid Prototyping Journal, Vol. 18 Issue 2, pp. 129 - 143, 2012.

# Sitography

## Past MFS missions and programs


[1] http://www.flightglobal.com/articles/2005/10/25/202326/down-sizing.html

[2] http://nmp.nasa.gov/ds1/

[3] http://nmp.jpl.nasa.gov/ds2/

[4] http://eo1.gsfc.nasa.gov/new/extended/sensorWeb/diagnosticTools.html

[5] http://nmp.nasa.gov/eo3/EDUCATION/mission.html

[6] http://www.sbir.gov/index.html

[7] http://www.designation-systems.net/dusrm/app3/mightysat.html

[8] http://directory.eoportal.org/presentations/129/12053.html

[9] http://www.qrg.northwestern.edu/projects/vss/docs/Mission/2-whats-where.html

[10] http://www.esa.int/esaMI/Aurora

[11] http://www.esa.int/TEC/Structures/SEMSMFWUP4F_0.html


## Heaters


[12] http://www.alper.it

[13] http://www.minco.com

[14] http://www.ricaheatingelements.com/homepage

[15] http://www.ptc-heater.com.tw

[16] http://www.conardcorp.com


## EMI/EMC solutions


[17] http://www.eastcoastshielding.com

[18] http://www.jabar.com

[19] www.p-p-t.co.uk

[20] www.mgchemicals.com

[21] http://www.rtpcompany.com

[22] http://www.ggi-international.compbox

## Sensors and buses

[23] http://www.i2cbus.com

[24] http://www.partssource.com

[25] http://www.moxa.com

[26] http://www.maxim-ic.com

[27] http://www.sensorsmag.com/

[28] http://www.ultracorinc.com/

## Others

[29] http://ocw.mit.edu/index.htm

[30] http://sitemaker.umich.edu/csdl

[31] http://www.flxsys.com

[32] http://adsabs.harvard.edu/

[33] http://www.esa.int/

[34] http://esmat.esa.int

[35] http://www.esacademy.com

[36] http://industrial-printing.net/

[37] http://www.epanorama.net

[38] http://www.apgasket.com

[39] http://www.rogerscorp.com

[40] http://en.wikipedia.org

[41] http://www.allflexinc.com

[42] http://www.flexiblecircuits.net

[43] http://www.epectec.comdf

[44] http://www2.dupont.com

[45] http://www.bestfpc.com

# Acknowledgments

I wish to thank everybody who was instrumental in making these three years a successful experience.

The first thought goes to all my mentors, since every one of them taught me things that I will always remember. Prof. Paolo Maggiore, Eng. Enrico Sacchi, Eng. Gaetano Poidomani, and Eng. Donald Schatzel: they gave me useful technical advices, but also many valuable lessons for my professional and personal life.

I have a debt of gratitude for all the experienced and skilled people that I met in Thales Alenia Space and at the Jet Propulsion Lab. I will not name anyone in particular, because I cannot name them all: the list would be very long, I might leave someone out and it wouldn't be fair. All of them have welcomed me in the best possible way, and helped me with their competence and professionalism. They have my warmest gratitude, and I hope we will work together again in the future.

I would also like to mention all the undergraduate students that worked with me, because my activity would have been incomplete without their contribution. I express my appreciation to Eng. Gianluca Filiddani, Eng. Alessandro Mannarelli, Eng. Antonio Iurlaro, and Eng. Michele Cencetti.

I need also to spend a few words for all my fellows and friends, both in Italy and in California, who worked, had fun, suffered, and rejoiced with me. Because of them I have the happiest memories of my Ph.D.

As usual, I save the last mention for those people who come first in my life. My family has always supported me, cheered me in good times and comforted me in bad times: they gave me the strength and motivation to go through all this. Gian Paolo has always been present to offer his advice, even when I was not willing to accept it. He gave me guidance and understanding, he shared his time and knowledge with me, he was able to make me recognize all the things in life that are more precious and essential than work.

Many thanks to all of you.

*Vorrei ringraziare tutti coloro che sono stati fondamentali nel trasformare questi tre anni in un'esperienza vincente.*

*Il primo pensiero va a tutti i miei tutori, perché ognuno di loro mi ha insegnato cose che ricorderò per sempre. Prof. Paolo Maggiore, Ing. Enrico Sacchi, Ing. Gaetano Poidomani ed Ing. Donald Schatzel: da loro ho ricevuto utili consigli tecnici, ma anche valide lezioni per la mia vita professionale e privata.*

*Ho un debito di riconoscenza verso tutte le persone esperte ed erudite che ho incontrato in Thales Alenia Space e al Jet Propulsion Lab. Non nominerò nessuno in particolare, perché non posso fare il nome di tutti: l'elenco sarebbe troppo lungo,*

*rischierei di lasciare fuori qualcuno e non sarebbe giusto. Tutti loro mi hanno accolta nel migliore dei modi e mi hanno aiutata con la loro competenza e professionalità. A loro va la mia gratitudine e spero che in futuro avremo ancora modo di lavorare insieme.*

*Vorrei anche menzionare tutti i tesisti che hanno lavorato con me, perché la mia attività sarebbe stata incompleta senza il loro contributo. Dedico un apprezzamento all'Ing. Gianluca Filiddani, Ing. Alessandro Mannarelli, Ing. Antonio Iurlaro, ed Ing. Michele Cencetti.*

*Devo anche spendere qualche parola per tutti i colleghi e gli amici, sia in Italia che in California, che hanno lavorato, si sono divertiti, hanno sofferto e gioito con me. Grazie a loro ho messo da parte i più bei ricordi del mio Dottorato.*

*Come sempre, riservo l'ultima menzione per le persone che metto al primo posto nella mia vita. Sarò sempre grata alla mia famiglia, che mi ha incrollabilmente supportata, tifando per me nella buona sorte e confortandomi nella cattiva sorte: loro mi hanno dato la forza e la motivazione per arrivare fin qui. Altrettanto devo a Gian Paolo, che è stato sempre presente, offrendo aiuto e suggerimenti, anche quando io non ero disposta ad accettarne. Mi ha dato consigli e comprensione, ha condiviso con me tempo e sapere, ma soprattutto è stato capace di farmi apprezzare tutto ciò che, nella vita, è più prezioso e prioritario del lavoro.*

*Ad ognuno di voi: grazie.*

*And I tell you, if you have the desire for knowledge and the power to give it physical expression, go out and explore. If you are a brave man you will do nothing: if you are fearful you may do much, for none but cowards have need to prove their bravery. Some will tell you that you are mad, and nearly all will say, 'What is the use?' For we are a nation of shopkeepers, and no shopkeeper will look at research which does not promise him a financial return within a year. And so you will sledge nearly alone, but those with whom you sledge will not be shopkeepers: that is worth a good deal. If you march your Winter Journeys you will have your reward, so long as all you want is a penguin's egg.*

Apsley Cherry-Garrard, The Worst Journey in the World